2006-07-20

Optimization of Active Noise Control for Small Axial Cooling Fans

Brian B. Monson
Brigham Young University - Provo

OPTIMIZATION OF ACTIVE NOISE CONTROL FOR SMALL AXIAL COOLING FANS

by

Brian B. Monson

A thesis submitted to the faculty of

Brigham Young University

in partial fulfillment of the requirements for the degree of

Master of Science

Department of Physics and Astronomy

Brigham Young University

August 2006

BRIGHAM YOUNG UNIVERSITY

GRADUATE COMMITTEE APPROVAL

of a thesis submitted by

Brian B. Monson

This thesis has been read by each member of the following graduate committee and by majority vote has been found to be satisfactory.

Date	Scott D. Sommerfeldt, Chair
Date	Timothy W. Leishman
Date	Jonathon D. Blotter
Date	Clayne W. Robison

BRIGHAM YOUNG UNIVERSITY

As chair of the candidate's graduate committee, I have read the dissertation of Brian B. Monson in its final form and have found that (1) its format, citations, and bibliographical style are consistent and acceptable and fulfill university and department style requirements; (2) its illustrative materials including figures, tables, and charts are in place; and (3) the final manuscript is satisfactory to the graduate committee and is ready for submission to the university library.

Date

Scott D. Sommerfeldt
Chair, Graduate Committee

Accepted for the Department

Ross L. Spencer
Graduate Coordinator
Department of Physics and Astronomy

Accepted for the College

Thomas W. Sederberg
Associate Dean
College of Physical and Mathematical Sciences

ABSTRACT

OPTIMIZATION OF ACTIVE NOISE CONTROL

FOR SMALL AXIAL COOLING FANS

Brian B. Monson

Department of Physics and Astronomy

Master of Science

Previous work has shown that active noise control is a feasible solution to attenuate tonal noise radiated by small axial cooling fans, such as those found in desktop computers. One such control system reduced noise levels of a baffled 80-mm fan in the free field with four small loudspeakers surrounding the fan. Due to industry specified spatial constraints, a smaller fan and speaker configuration was desirable. The smaller configuration maintains similar control performance, further facilitating practical implementation of the control system. The smaller control system employs a smaller fan running at a higher speed. Different loudspeaker configurations for control exist and have been tested. A configuration consisting of four control sources spaced symmetrically around and coplanar to the fan exhibits global control of the tonal component of the fan noise. A configuration with three symmetrically spaced sources is

shown to perform similarly, agreeing with theoretical prediction. An analysis of the control system in a non-ideal reflective environment is also discussed.

ACKNOWLEDGEMENTS

I wish to express my sincere gratitude to the following individuals, without whom this work would not have been accomplished:

- Scott D. Sommerfeldt, for his guidance, mentoring, and friendship
- Timothy W. Leishman, for his regard for my future
- Jonathon D. Blotter, for his insight
- Kent L. Gee, for his willingness to continue to help
- Benjamin M. Faber, for teaching me
- Connor Duke, for his work and for helping me want to work (and laugh)
- Cole Duke, Megan Parker, and Patty Thomas, for their diligence
- Dave Nutter, Sarah Rollins, and Matt Gee, for their help and patience
- The BYU Acoustics Research Group, for their support
- Diann Sorensen and Nan Ellen Ah You, for their information and preparation
- Angela, Scott, Derek, Elise, and Andrew, for their love
- My mother and father, for good parenting (and everything listed above)
- God, Who gives us our abilities and our opportunities

TABLE OF CONTENTS

LIST OF FIGURES

Chapter 2

Chapter 3

Chapter 4

Appendix A

CHAPTER 1

INTRODUCTION

1.1 Cooling Fan Noise

The control of noise radiated by small axial cooling fans has received some recent scientific attention, particularly with regard to fans found typically in standard electronic office equipment, such as desktop computers. Noise radiated from these fans is often found in the workplace, the home, and the classroom. Such noise can be disturbing or distracting and cause unnecessary annoyance. While these noise levels are typically not high enough to cause permanent hearing damage, a study performed by Evans and Johnson at Cornell University[1] showed that prolonged exposure to even low levels of office noise can be detrimental to health and well being. Thus, an effective solution to this fan noise problem is needed.

1.2 Active Noise Control

Methods of noise control have traditionally been separated into two categories: passive noise control and active noise control. Passive techniques of noise control most often attempt to eliminate noise propagation to a listener by introducing a sound-reducing barrier or path of some sort between the source and the listener. Perhaps the simplest and most common example of passive noise control is the practice of "plugging" one's ears to block out loud sounds.

In contrast, active noise control (ANC) may be defined as the deliberate introduction of a secondary sound source to eliminate at some location the undesired

sound radiated by a noise source. The sound reduction in this case happens within the medium of propagation (i.e., air), and without the aid of any physical barrier.

Though the concept of ANC may seem somewhat foreign to many, it was first conceived and patented by the German scientist Paul Lueg in 1936.[2] Lueg's experimental attempts of ANC were apparently unsuccessful. The application of ANC apparently did not catch on quickly, as little was heard about it again until 1953. In that year, Olson and May[3] proposed an "electronic sound absorber" that could be used in a room to cancel low frequency "spot noise" around a listener's head. Because of the difficulty of implementation, however, the full potential of ANC was not realized until decades later. Most recently, advances in digital signal processing have greatly enhanced the capabilities of computer processors to successfully execute the advanced control algorithms necessary for an effective ANC system. Thus, ANC technology is now being considered as a possible solution to many common noise problems.

1.3 Active Noise Control of Cooling Fans

ANC has become an attractive solution for the reduction of fan noise, particularly with the tonal component of the noise. Notable efforts have been made to combat the axial fan noise problem in the free field with some successful results. Quinlan[4] achieved global sound power reductions of 12 dB for the fundamental frequency of the fan noise tonal component, and 7 dB for the second harmonic. His method used a single secondary control source loudspeaker placed next to a fan in a baffle. Wu[5] showed confirming results, using a procedure similar to Quinlan's. Lauchle *et al.*[6] utilized the fan itself as the secondary control source, using the fan as a shaker-mounted actuator. This resulted in sound power reductions of 13 and 8 dB for the fundamental frequency and second

harmonic, respectively. Homma *et al.*[7] included the addition of a duct and multiple control sources, combining active and passive means of fan noise control. Their method exhibited reduction of both the tonal and broadband noise components, with an overall sound power reduction of 4.9 dB.

A study performed by Gee and Sommerfeldt[8] showed that multiple control sources surrounding a fan exhibited global noise reduction of the fundamental frequency and multiple harmonics. The study reported spatially averaged squared pressure reductions of 10.1 dB, 16.1 dB, and 12.8 dB for the fundamental, second harmonic, and third harmonic, respectively. This control system was based on a multi-channel version of the filtered-x LMS control algorithm developed by Sommerfeldt.[9]

There are two points of particular significance in the control approach taken by Gee and Sommerfeldt that distinguish it from previous work: (1) multi-channel adaptive control with sources coplanar to the fan and (2) near-field error sensor placement as a stable method of fan noise control. Their study further proposed that an optimal location for the error sensors existed coplanar to the fan and control actuators, such that optimum global control could be achieved. The research done by Gee and Sommerfeldt was the basis for the current research.

1.4 Overview of Research

The system developed by Gee needed optimization with real-world conditions and specified industry constraints. Efforts are being made to decrease the size of electronic office equipment (e.g. desktop computers), which often contain at least one axial cooling fan. The control system size, including actuators and all electronic hardware, should therefore be minimized to comply with the decreased sizes. It was expected that the

system would still be able to function properly, despite these limitations. The proposed research aimed to assess the validity of this expectation.

All measurements performed by Gee were in a free-field (anechoic) environment. In contrast, a typical office environment is enclosed and often highly reflective in nature. The control system therefore needed testing for feasibility in an office-type setting. As part of the experimental testing procedure, true sound power measurements were desired to quantify the control system performance, and to validate the spatially averaged squared pressure reductions reported by Gee and Sommerfeldt.

Optimization of the control system also included the need for optimization of the miniature loudspeaker response. Gee reported poor low-frequency loudspeaker response as detrimental to control system performance.[8] An examination of the miniature loudspeaker enclosures was needed.

While Gee examined several control system configurations, an analysis of three control sources spaced symmetrically around the fan was not tested. This configuration has been studied in theory, and an experimental verification was deemed beneficial for this research. The main objectives of the research were divided into the following specific tasks:

- Decrease the fan and control loudspeaker size
- Determine ideal error microphone placement for the small system
- Optimize the miniature loudspeaker enclosures
- Achieve global noise control in a free field
- Examine the effects of changing control source configurations
- Achieve global control in a reflective environment

- Maintain comparable airflow with the small fan

It was anticipated that the success of these objectives would enhance the efficacy of ANC as it relates to axial fans and put it one step closer to widespread practical implementation. The success of ANC for axial fans would benefit anyone who works with or around a desktop computer, or any other electronic equipment that houses an axial cooling fan.

1.5 Thesis Organization

Chapter 2 presents the main points of theory used in this research, including a description of fan noise and several principles involved in ANC. The method and experimental setup used to complete the research objectives are discussed in Chapter 3. The results of the experimental tests are presented in Chapter 4. Chapter 5 finishes with conclusions of the research and recommendations for future research.

CHAPTER 2

THEORY

2.1 Fan Noise

Fan noise is characterized acoustically by discrete tones superposed on a broadband spectrum, as can be seen in Figure 2.1. The broadband component of the noise has been attributed to unsteady time-variant fluid loading on the blades of the fan as they rotate,[6] as well as vortices generated at the tips and trailing edges of the fan blades.[10] Tonal fan noise is caused by unsteady time-invariant fluid loading on the rotating fan blades. The latter may be ascribed to the placement of stationary flow obstructions near the inlet or exhaust of the fan, such as stators or finger guards. The tones present in the fan noise spectrum are found to be harmonically related to each other, and directly related to the rotational speed of the fan. The first major tone, referred to as the blade passage frequency (BPF), often lies between 100 and 600 Hz for cooling fan applications. The BPF generally exhibits the highest radiation level. It is calculated from revolutions per minute (RPM) as

$$BPF = N \times \frac{RPM}{60}, \tag{2.1}$$

where N is the number of blades on the fan. While both noise components mentioned are present in the spectrum of cooling fan noise, the tonal component often dominates the overall sound pressure level and perceived noise level.[11] It has therefore been the emphasis of most studies on fan noise control.

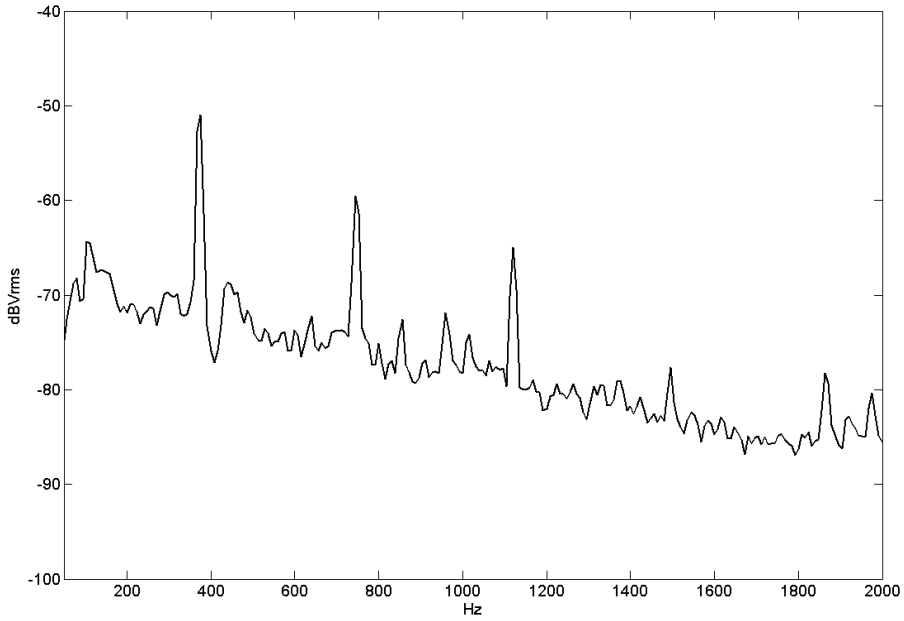

Figure 2.1 A typical power spectrum of fan noise consisting of both broadband and tonal noise.

2.2 Mutual Coupling

The early efforts using ANC made by Lueg and Olson were based on the principle of destructive interference in wave superposition. The most significant limitation of using only destructive interference is that the control of noise is specific to local regions (i.e., around a listener's head) and may actually cause an increase of noise in one or more locations elsewhere in the environment.

An additional mechanism of active sound cancellation relies upon mutual impedance coupling. Typically, if the principle of strong mutual coupling can be employed in the active control of a noise source radiating into free space, the resulting control behavior is of a global nature, and is therefore more desirable. A brief summary of mutual coupling follows.

As two monopole sources radiating into free space are brought into near-field proximity with one another, the mutual impedance seen by each source is modified due to the presence of the other source.[12,13] The total power, W, radiated by both sources is determined analytically to be

$$W = \frac{k^2 \rho c}{8\pi} |Q_1|^2 \left(1 + A^2 + 2A \frac{\sin kd}{kd} \cos\gamma\right), \tag{2.2}$$

where

$$\frac{Q_2}{Q_1} = Ae^{j\gamma}, \tag{2.3}$$

k is the acoustic wave number, ρ is the density of the medium (kg/m^3), c is the speed of sound (m/s), and d is the separation distance (m) between the two sources. The variables Q_1 and Q_2 represent the monopole source strengths. Optimizing the secondary source strength, Q_2, relative to the primary source strength, Q_1, and minimizing the above equation leads to the minimum power radiated by both sources,

$$W_{MIN} = \frac{k^2 \rho c}{8\pi} |Q_1|^2 \left[1 - \left(\frac{\sin kd}{kd}\right)^2\right]. \tag{2.4}$$

The optimum secondary source strength, Q_2, to achieve the minimum power radiation is found to be

$$Q_2 = -Q_1 \frac{\sin kd}{kd}. \tag{2.5}$$

The expression in Eq. (2.4) is seen to differ slightly from the radiated power of a dipole due to the manipulation of the secondary source strength. On the right side of Eq. (2.4) is seen the expression representing the power radiated by a single monopole source (W_{MONO}) of strength Q_1, so that W_{MIN} may also be expressed as

$$W_{MIN} = W_{MONO} \left[1 - \left(\frac{\sin kd}{kd}\right)^2\right]. \tag{2.6}$$

Extending this secondary source optimization technique to a system consisting of two, three, and four symmetrically spaced secondary sources in a plane, as shown in Figure 2.2, gives the minimum radiated power for each configuration. The results of this analysis have been studied by Nelson and Elliott[12] and Gee[14], and are shown in Figure 2.3, in which the minimum power radiation, relative to the power radiated by a single monopole, is plotted as a function of kd. Figure 2.4 shows the resulting optimum secondary source strengths relative to the primary source strength for each case.

From Figure 2.3 it can be seen that as kd becomes very small, radiated power is greatly decreased, whereas kd approaching π leads to very little or no reduction of radiated power. As kd becomes small there also appears to be very little difference in the curves depicting the attenuation for three and four secondary sources. (Increasing the number of secondary sources to greater than four tends to bring little gain in sound power attenuation for all values of kd.[14])

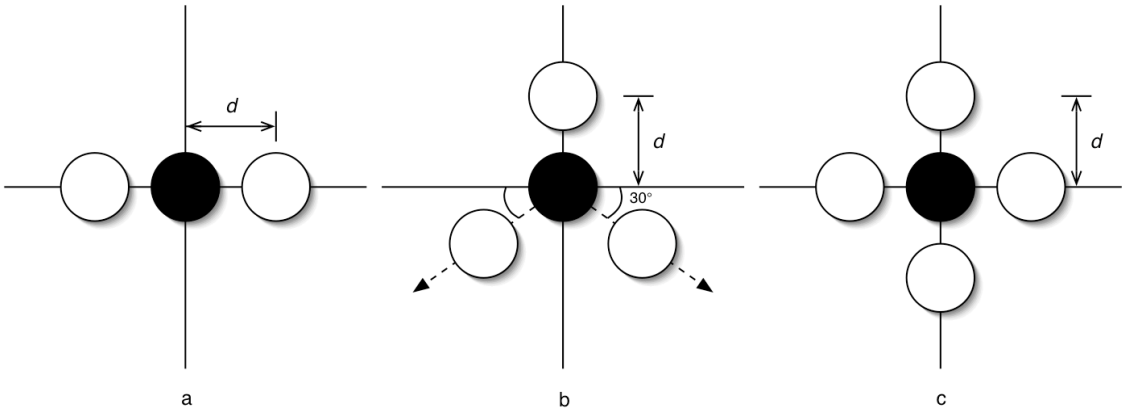

Figure 2.2 Control source configuration for (a) two control sources, (b) three control sources, and (c) four control sources on a plane.

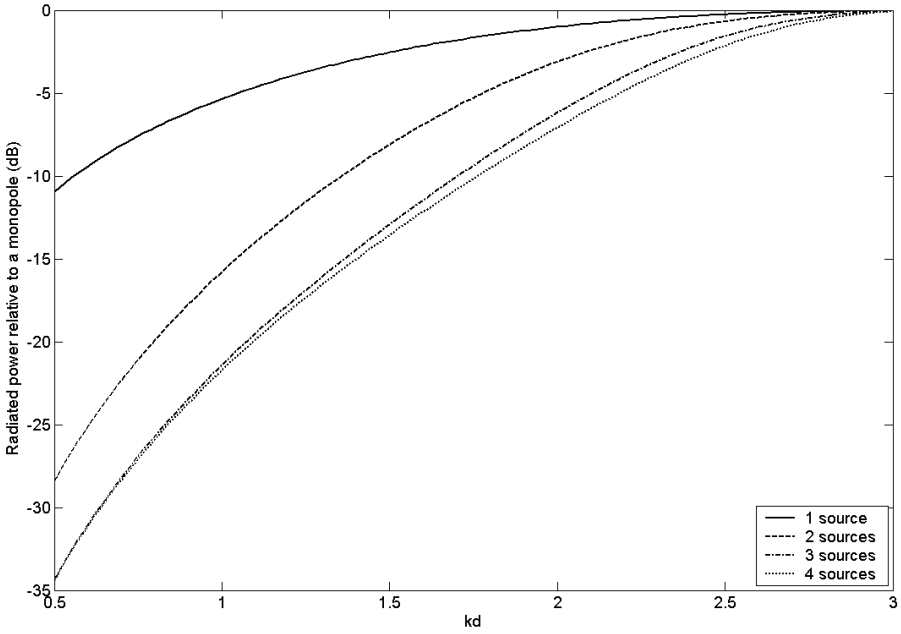

Figure 2.3 Minimum radiated power for control source arrangements of one, two, three, and four symmetrically spaced sources.

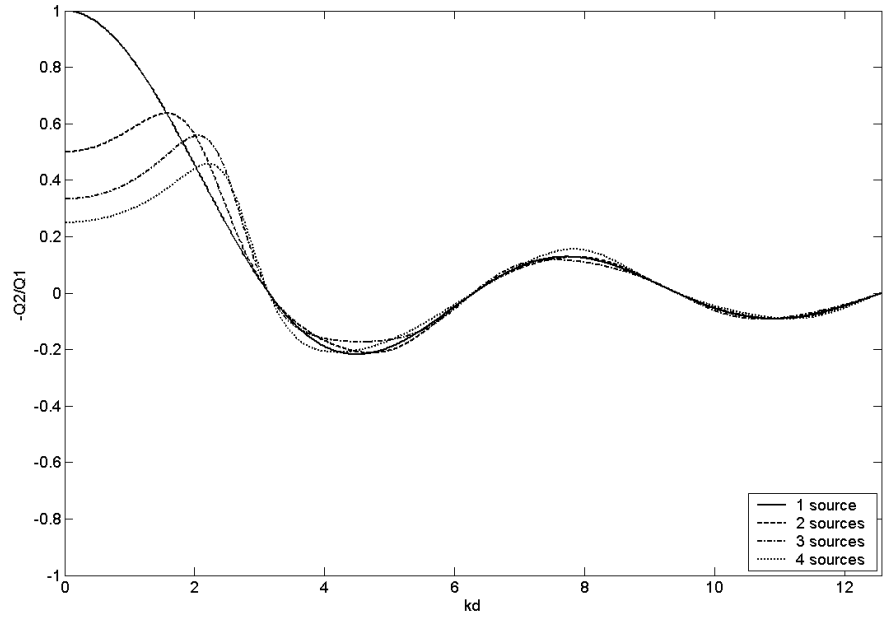

Figure 2.4 Optimal secondary source strengths for control source arrangements of one, two, three, and four symmetrically spaced sources.

2.3 Error Sensor Location

To obtain the optimum control shown in Figure 2.3 in an experimental setting requires one to recreate the sound field that exists when the minimum sound power radiation is achieved. From the analysis given in the previous section, the secondary source strengths were used to simulate the controlled sound field attained when sound power radiation is minimized. All sources were modeled as point sources in free space using Green's functions for wave propagation. This simulation technique followed that developed by Gee.[15]

Figures 2.5 and 2.6 show the optimally controlled sound field in the source plane (control plane) created by a simple primary (noise) source surrounded by four symmetrically spaced secondary (control) sources. Each plot shows the controlled pressure field in dB relative to the pressure field of a single noise source. The dark closed contour represents a pressure null. This null shape varies slightly depending upon the value of *kd*, which is dependant on frequency and the separation distance between the noise source and control sources (see Figure 2.2).

Figures 2.5 and 2.6 show different frequency cases of 600 Hz and 1800 Hz, respectively, each with a separation distance of $d = 0.045$ m. The primary noise source is located at the position (0, 0). The control sources are situated around the noise source and are indicated by the regions of increased intensity at 45, 135, 225, and 315 degrees. A comparison of the two plots shows the slight change in the pressure null pattern with the increase of frequency. Figures 2.7 and 2.8 show these same frequencies in the control plane with three symmetrically spaced control sources. The three control sources are located at 90, 210, and 330 degrees around the noise source.

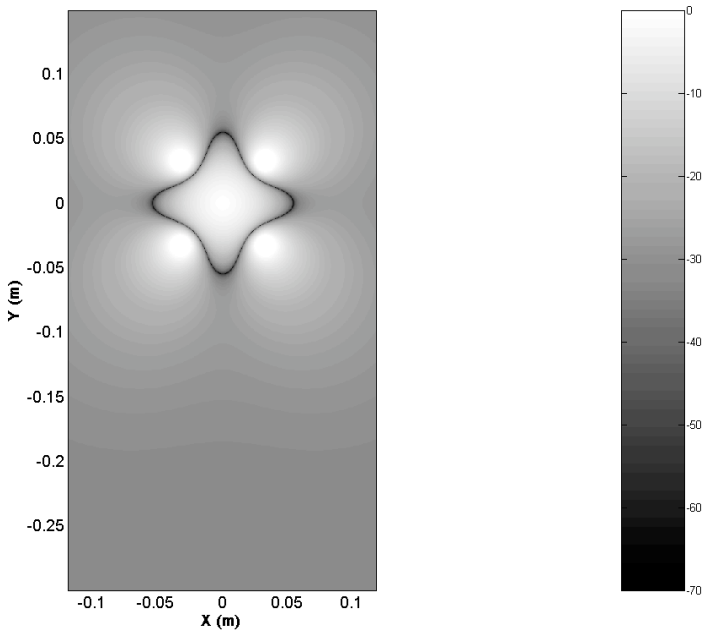

Figure 2.5 Controlled pressure field coplanar to the noise source and four secondary sources – 600 Hz.

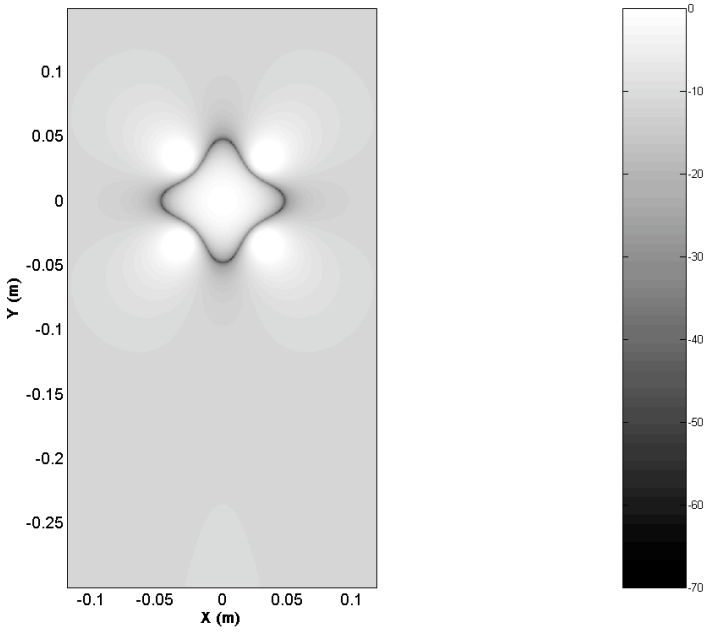

Figure 2.6 Controlled pressure field coplanar to the noise source and four secondary sources – 1800 Hz.

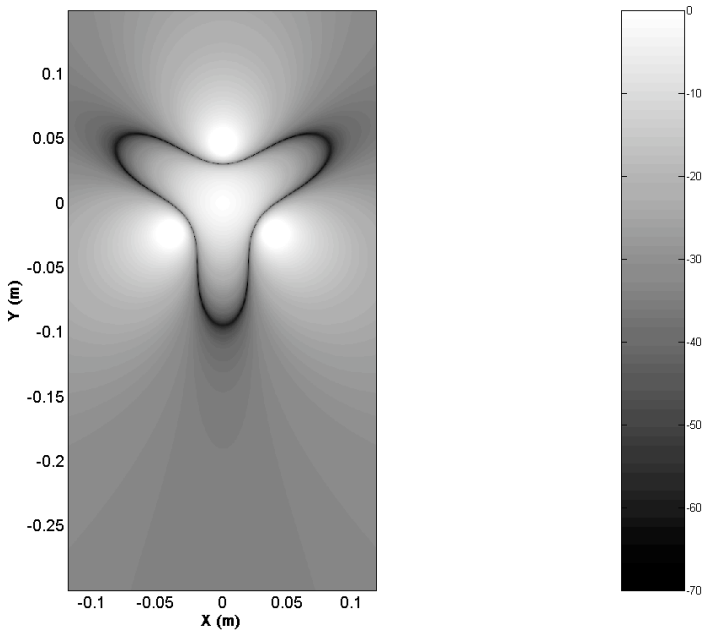

Figure 2.7 Controlled pressure field coplanar to the noise source and three secondary sources – 600 Hz.

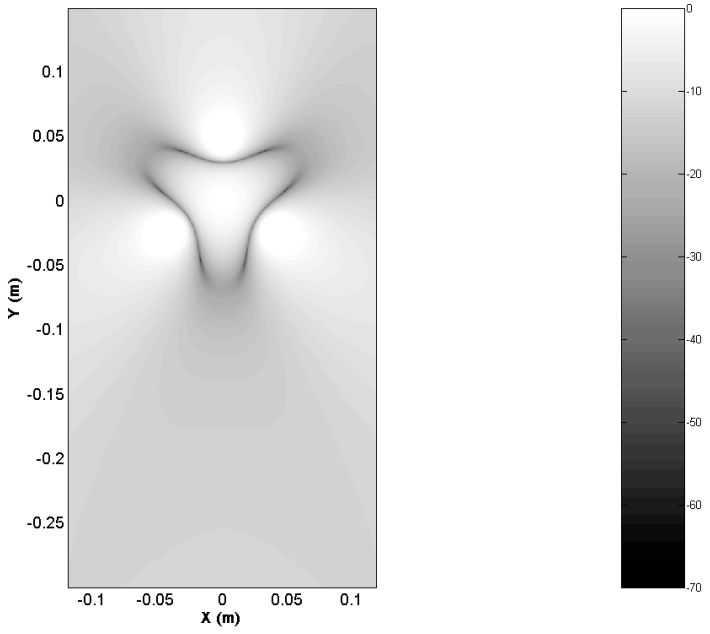

Figure 2.8 Controlled pressure field coplanar to the noise source and three secondary sources – 1800 Hz.

The shape of the null pattern tends to deform somewhat as it is extruded away from the control plane. Its behavior is shown in Figure 2.9 for the case of four secondary sources and in Figure 2.10 for three secondary sources. In both cases it is seen that the shape of the null contour becomes increasingly circular away from the control plane. The spreading of the null contour in the x and y directions appears to be linear in nature, particularly in the far field, as can be seen in Figure 2.11.

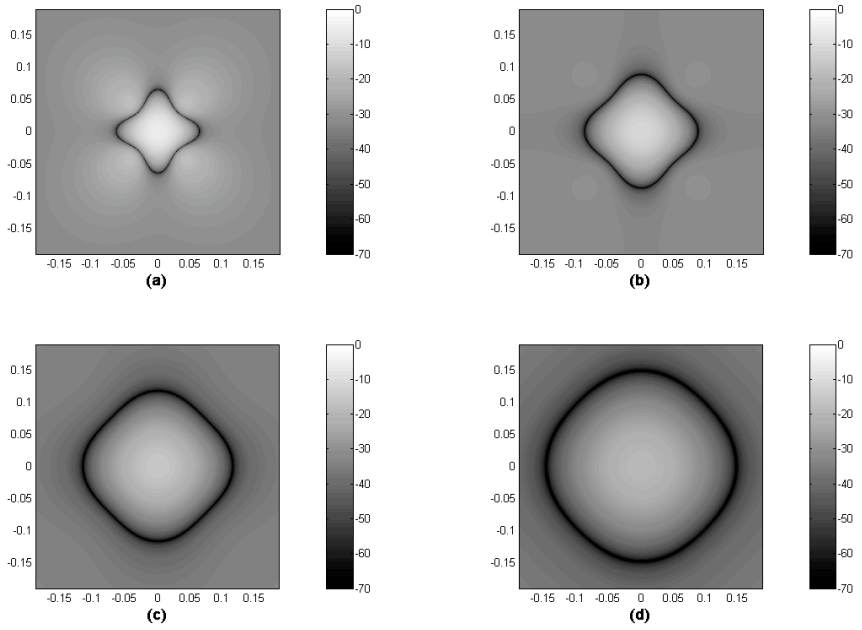

Figure 2.9 Controlled pressure field at (a) 2.5 cm (b) 5 cm (c) 7.5 cm and (d) 10 cm above the control plane for 600 Hz noise with four control sources.

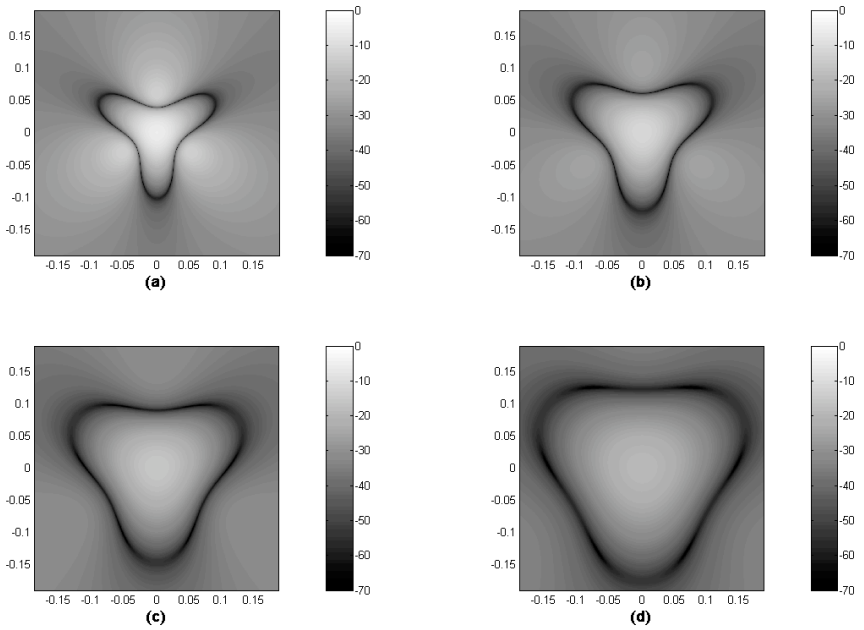

Figure 2.10 Controlled pressure field at (a) 2.5 cm, (b) 5 cm, (c) 7.5 cm, and (d) 10 cm above the control plane for 600 Hz noise with three control sources.

Figure 2.11 shows the acoustic far-field behavior of the null pattern in the x-z plane for the three-source case, where z is the direction perpendicular to the control plane. The control plane is located in the x-y plane (z = 0) so that the null pattern in this diagram spreads above and below the control plane. As can be seen, the null pattern spreads linearly at a constant angle off of the control plane. Based on the assumption of acoustic far-field behavior, it has been shown that this angle of spreading can be calculated analytically as

$$\theta = \arcsin\left\{\frac{2\sqrt{3}}{3kd}\arccos\left[\frac{1}{2}\left(\left(\frac{\frac{\sin kd}{kd}}{1+2\frac{\sin k\sqrt{3}d}{k\sqrt{3}d}}\right)^{-1}-1\right)\right]\right\}, \tag{2.7}$$

where θ is measured from the z-axis toward the control plane.[16]

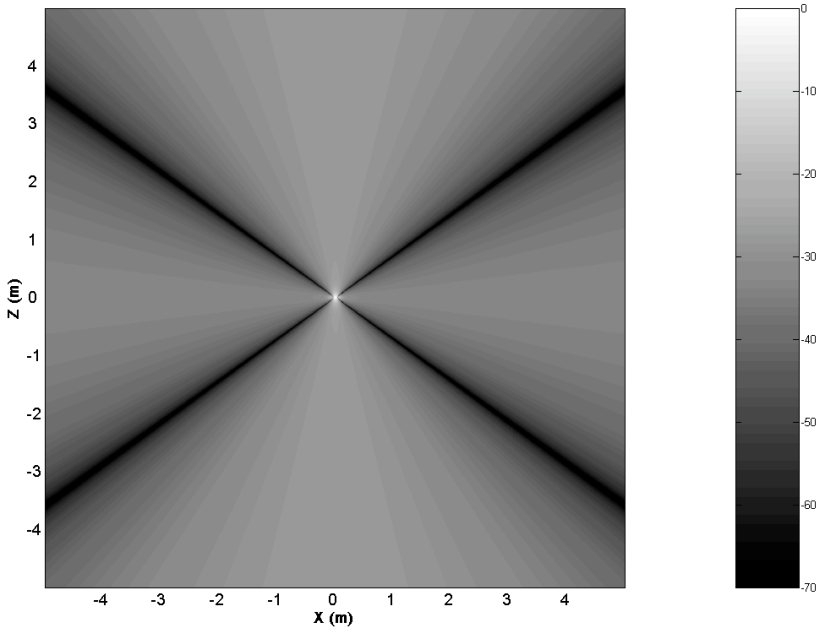

Figure 2.11 Controlled pressure field for three secondary sources showing the x-z plane in the acoustic far-field (control plane located at z = 0).

The far-field analysis results in a null pattern that is found only on this angle of spreading, suggesting that null points would only be found off of the plane containing the sources. Figure 2.11 seems to agree with this hypothesis. Viewing the near-field behavior, however, shows that the null pattern does indeed penetrate the control plane, as can be seen in Figure 2.12. The discrepancy of the two analyses may be due to the far-field assumption.

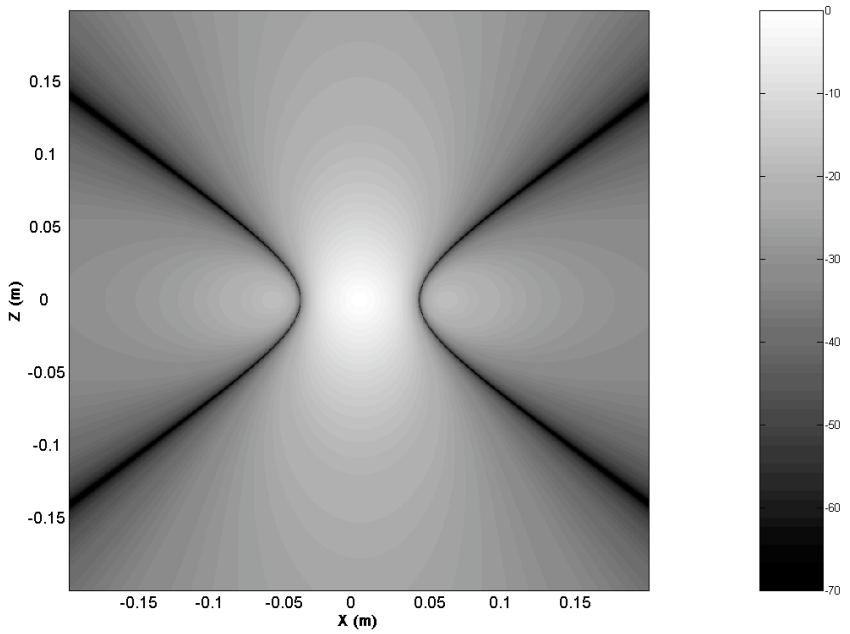

Figure 2.12 Controlled pressure field for three secondary sources showing the x-z plane in the acoustic near-field.

Close attention should be paid to the pressure null pattern because of its significant role in attempting to recreate the controlled sound pressure field in practice. From the earliest efforts of Lueg in the 1930s, ANC was implemented with the aid of a microphone (now commonly termed an "error sensor") placed at some location in the noisy environment. The secondary source was then used to cancel the noise at that error sensor. To accurately recreate the controlled fields shown in Figures 2.5 through 2.8, an error sensor or multiple error sensors can be placed at a point or multiple points located along the pressure null. The secondary sources can then be used to minimize the noise signal at the error sensors, thereby recreating the pressure null pattern, and, therefore, the controlled pressure field.

It has been found that the error sensor microphone placement may be optimized by finding the regions of greatest pressure attenuation when the global sound power radiation is minimized.[13] Analysis was performed to determine whether or not the null contour found on the control plane was in fact the region of greatest pressure attenuation in the controlled pressure field.

Figure 2.13 shows the maximum theoretical attenuation achieved by the four-control source system in the pressure null extruded from 0 to 3 m above the control plane in the x = 0 plane. The attenuation in the far field (z = 3 m) is seen to be much greater than that achieved on the control plane. The attenuation achieved varies with respect to the azimuthal angle ϕ (see Figure 2.14), and this variation is shown in Figure 2.15. Here the attenuation is shown from the control plane to the far field with 5-degree increments in ϕ. A similar trend is seen in all cases. (Figure 2.13 is the $\phi = 0$ case.)

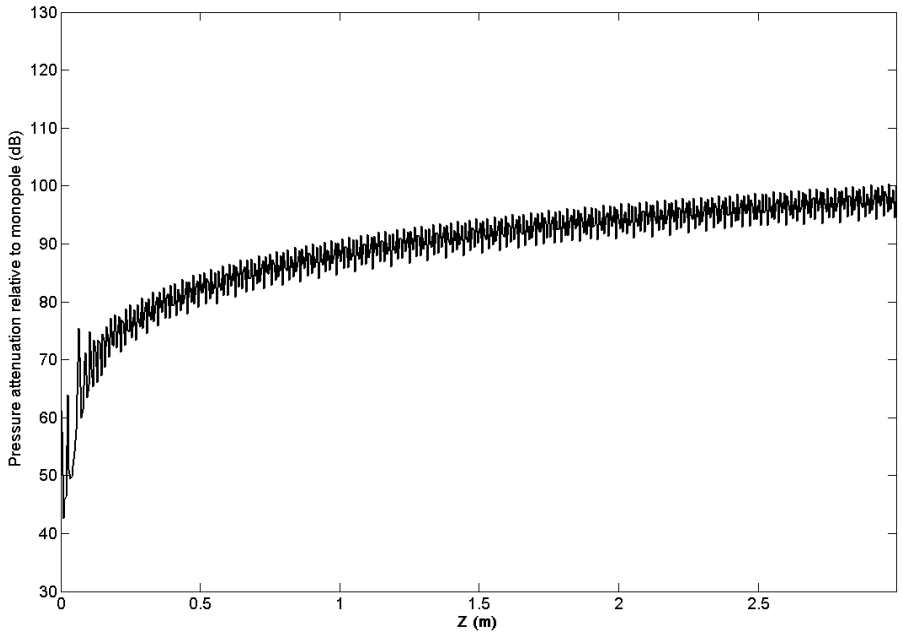

Figure 2.13 Maximum attenuation achieved in the z-direction for four control sources (far-field).

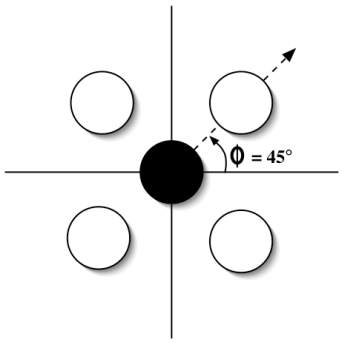

Figure 2.14 Four-control source configuration showing azimuthal angle ϕ.

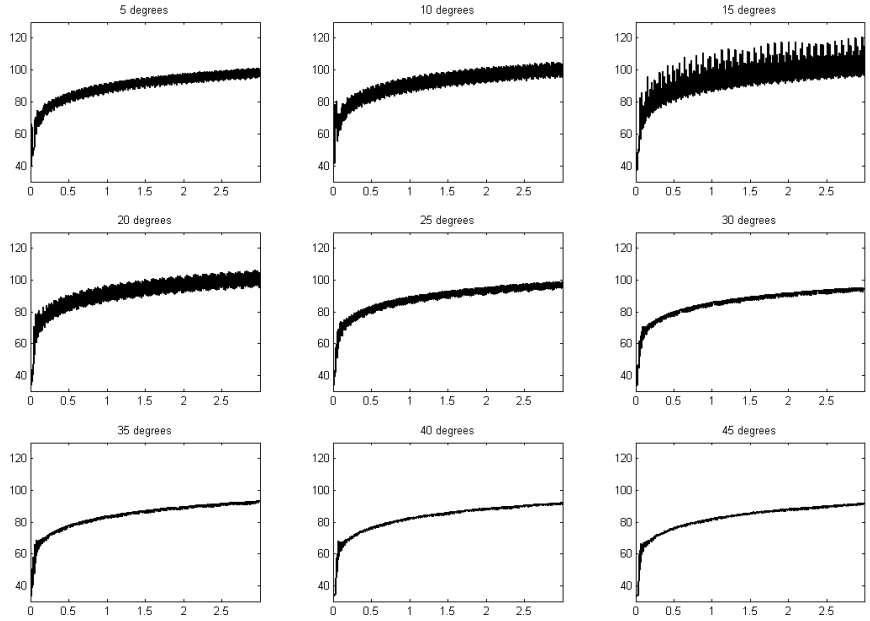

Figure 2.15 Maximum attenuation achieved in the z-direction for four control sources, showing the change in attenuation with rotation in ϕ (far-field).

This suggests that error sensor microphones placed in the far field would lead to the greatest sound power attenuation globally. In practice, however, this may not be feasible in an office environment. Constraining the previous analysis to the acoustic near field results in the attenuation shown in Figures 2.16 and 2.17. Again, Figure 2.16 shows the x = 0 plane (ϕ = 0), while Figure 2.17 shows changes in maximum attenuation with

rotation in the azimuthal direction. Here the distance is limited to 4 cm above the control plane (perhaps a more practicable distance for error sensor placement).

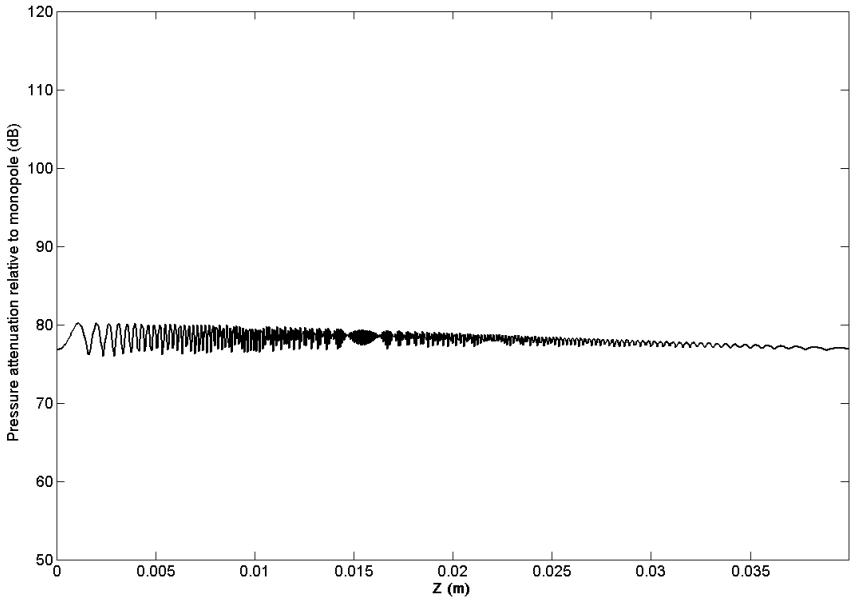

Figure 2.16 Maximum attenuation achieved in the z-direction for four control sources (near-field).

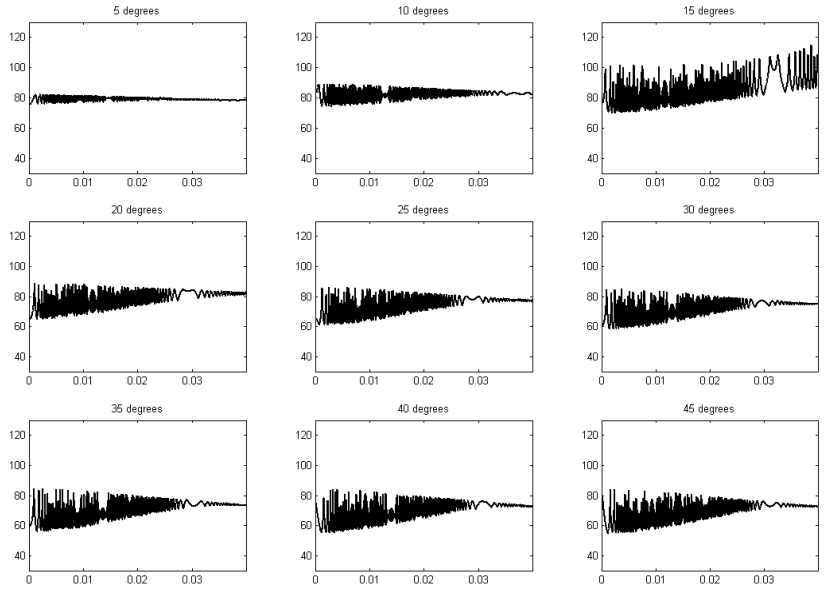

Figure 2.17 Maximum attenuation achieved in the z-direction for four control sources, showing the change in attenuation with rotation in ϕ (near-field).

The attenuation achieved within 3 cm off of the plane varies greatly and appears to be extremely sensitive to location. At some angles the difference in attenuation is as much as 30 dB, depending on exact location of the error sensor. After 3 cm the attenuation becomes more consistent, suggesting that more stable error locations can be found more than 3 cm above the control plane. It is interesting to note, however, that at some angles the attenuation achieved on the plane is comparable to or greater than that achieved at 4 cm (e.g. 0 degrees, 5 degrees, 10 degrees, 40 degrees, and 45 degrees). In practice, the ideal error sensor locations depend on many factors, as will be explained in section 4.1.1. For the purposes of this research, the error sensor locations will be constrained to the control plane. Thus, the term "optimal" will be used to refer to control source configurations and results where the error sensors were located only along the pressure null contour laying on the control plane.

2.4 The Multi-channel Filtered-x LMS Algorithm

To accomplish the task of recreating the null pattern, a robust control algorithm was used which could successfully minimize the error sensor signals. The filtered-x least mean-square (LMS) algorithm has been used extensively in ANC applications. Its development is given as follows. For a more complete derivation of the algorithm, see references 9, 12, 13, and 15.

Figure 2.18 shows a block diagram for a control system using the single input, single output adaptive LMS control algorithm. In this diagram and throughout this section, the parameter n represents the sampled time variable and z represents the discrete-time frequency variable. The LMS algorithm, as shown here, is a feedforward control algorithm requiring a reference signal $x(n)$ that is correlated with the noise signal

sent to the environment $P(z)$. The function $W_n(z)$ represents the nth iteration of the transfer function of the adaptive filter used in the algorithm implementation, written as

$$W_n(z) = w_0 + w_1 z^{-1} \ldots w_N z^{-N}, \tag{2.8}$$

for $N + 1$ filter coefficients. The algorithm calls for an error signal,

$$e(n) = d(n) + u(n) = d(n) + \mathbf{w}_n \mathbf{x}(n)^T, \tag{2.9}$$

where $\mathbf{w}_n$ represents the vector containing the coefficients of the nth iteration of the filter transfer function $W_n(z)$,

$$\mathbf{w}_n = [w_0 \; w_1 \ldots w_N] \tag{2.10}$$

and $\mathbf{x}(n)$ is the vector containing the current and past samples of $x(n)$,

$$\mathbf{x}(n) = [x(n) \; x(n-1) \ldots x(n-N)]. \tag{2.11}$$

The error function is used to find the mean-square error (MSE), a function for which a minimum may be found. Locating the minimum is accomplished by the method of steepest descent.

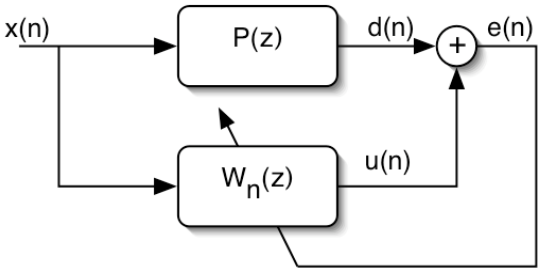

Figure 2.18 Block diagram for a single input, single output control system using the adaptive LMS algorithm.

The method of steepest descent uses the gradient to locate the extremum of some quadratic function (i.e., the MSE). The gradient of the quadratic function, which points in the direction of greatest ascent, may be subtracted iteratively in order to update the

transfer function of the adaptive filter. In practice, the gradient of the MSE is replaced by an estimate of the gradient, so that the filter update equation is given by

$$\mathbf{w}_{n+1} = \mathbf{w}_n - \mu e(n)\mathbf{x}(n). \tag{2.12}$$

The parameter μ constrains the step size taken at each iteration of the algorithm to locate the minimum of the quadratic function. It therefore controls how quickly the algorithm converges upon the minimum.

The block diagram shown in Figure 2.18 is a sufficient representation of a typical control system where all signals are transmitted directly through electronic lines. For ANC, however, the control signal, $u(n)$, is transmitted through an electroacoustic path before being summed with d to produce the error signal. In Figure 2.19, $H(z)$ represents the transfer function of the electroacoustic control path.

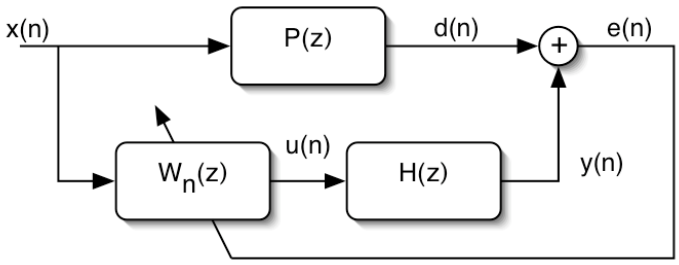

Figure 2.19 Block diagram of the LMS control system with an acoustic control path.

Because of the introduction of the control path, $H(z)$, the LMS algorithm requires modification for proper implementation with ANC. This modification is shown schematically in Figure 2.20. An estimate $\hat{H}(z)$ of the control path transfer function is inserted to filter the reference signal before it is sent through the LMS process. The filtered-x signal, $r(n)$, is then used to update to filter coefficients, so that the filter update equation becomes

$$\mathbf{w}_{n+1} = \mathbf{w}_n - \mu e(n)\mathbf{r}(n), \tag{2.13}$$

where $\mathbf{r}(n)$ is the vector containing the current and past samples of $r(n)$.

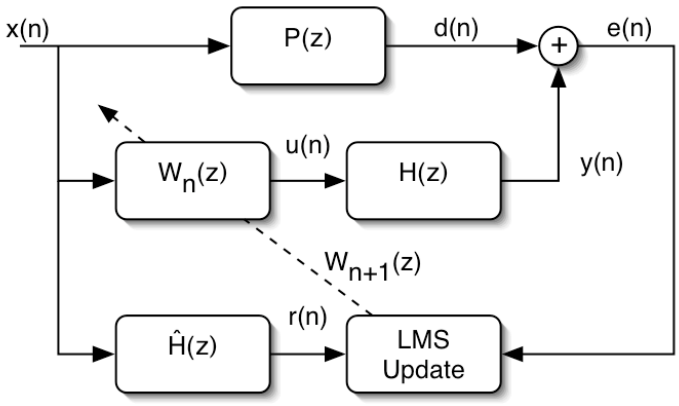

Figure 2.20 Block diagram of the single input, single output control system using the adaptive filtered-x LMS algorithm.

The process of determining an appropriate estimate of the control path is referred to as system identification. It can be accomplished by obtaining the frequency response from the point of control signal generation to the point of reception of the error signal. This is often accomplished with the aid of a random noise signal transmitted through the control path before the control process is begun. System identification performed in this manner is termed "offline" system identification and is based on the assumption that the control path is time invariant. If such is not the case, an "online" system identification method exists in which the estimate of the control path can be updated concurrently with the control filter update.

The final control algorithm used for this research requires only one change from that discussed to this point. The single input, single output control system can be adjusted slightly to incorporate single input, multiple output control if such is found to be

advantageous. Figure 2.21 shows the block diagram for a single input multiple output control system. The bold arrows indicate arrays of multiple signals.

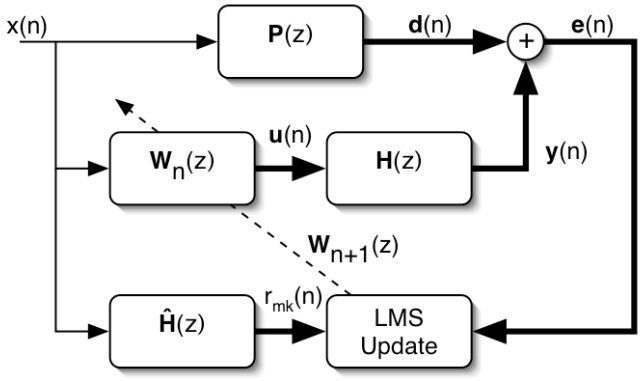

Figure 2.21 Block diagram of a single input, multiple output control system using the adaptive filtered-x LMS algorithm.

With multiple signals, assuming a total number of K control signals and M error signals, the mth error signal will contain contributions from each control signal, denoted $y_{mk}(n)$, and may now be written

$$e_m(n) = d_m(n) + \sum_{k=1}^{K} y_{mk}(n). \tag{2.14}$$

The signal $r_{mk}(n)$ is an array of signals consisting of the reference signal filtered with control path transfer functions from the kth control signal to the mth error signal. The final control filter update equation then becomes

$$\mathbf{w}_{k,n+1} = \mathbf{w}_{k,n} - \mu \sum_{m=1}^{M} \mathbf{r}_{mk}(n) e_m(n), \tag{2.15}$$

where $\mathbf{w}_{k,n}$ represents the kth vector containing the coefficients of the nth iteration of the filter transfer function, $\mathbf{W}_n(z)$, and $\mathbf{r}_{mk}(n)$ contains the past and current samples of $r_{mk}(n)$.

CHAPTER 3

METHOD

3.1 Fan Size

An 80-mm fan was used by Gee and Sommerfeldt,[15] which has been a standard size for desktop computer cooling applications. The fan with the control system embedded, however, requires an area of approximately 125 × 125 mm. With increasing efforts to decrease the size of desktop computers, a control and fan configuration that fits within the standard 80 × 80-mm area was desired for a more commercially viable system. The selection of a 60-mm DC fan was made to comply with this spatial constraint. The modification is illustrated in Figure 3.1.

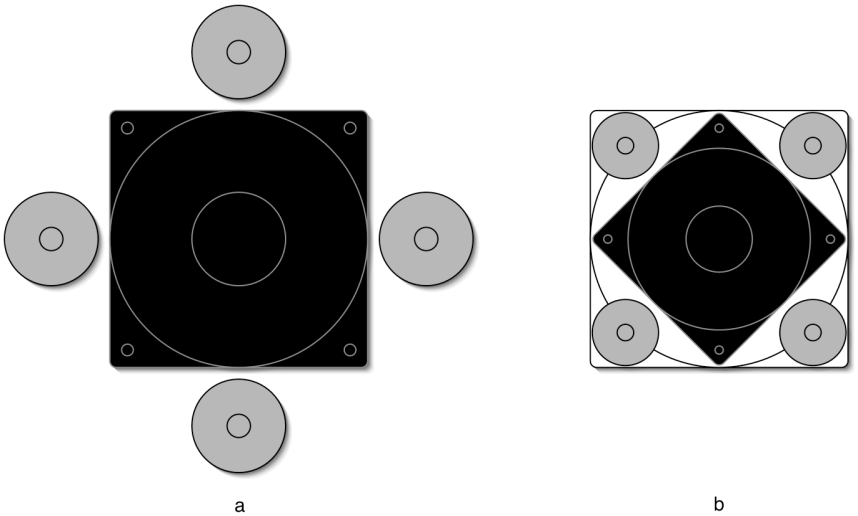

Figure 3.1 Schematic of size modifications made from (a) the existing 80-mm fan control system to (b) the 60-mm fan control system.

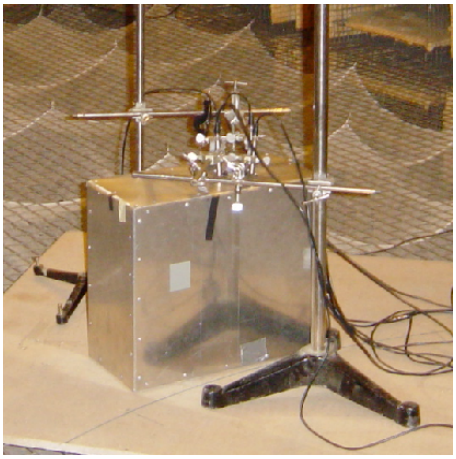

Figure 3.2 An aluminum mock computer casing containing a fan and control system.

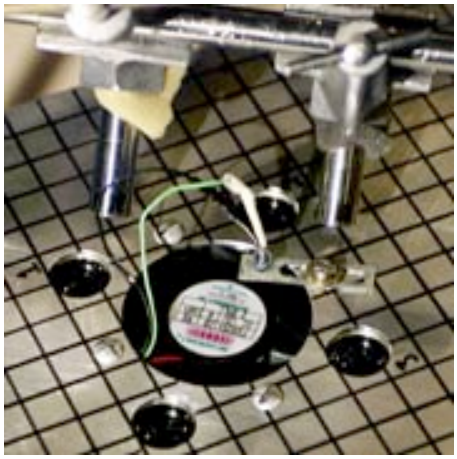

Figure 3.3 A 60-mm fan with miniature control loudspeakers.

A mock computer casing, shown in Figure 3.2, was used for experimental testing. The casing was 0.45 m in height, 0.4 m in length, and 0.25 m in width. The 60-mm fan used in the top of the casing was a Mechatronics F6025X DC cooling fan (see Figure 3.3). Four 20-mm diameter Regal Electronics R-20-E miniature loudspeakers were selected as control actuators. They were spaced symmetrically around the 60-mm fan, fitting within an 80 × 80-mm area, with a separation distance (from the center of the fan to the center of each loudspeaker) of $d = 0.045$ m. Such miniature loudspeakers typically present a problem in that their low frequency response is generally poor, and the input voltage to the loudspeakers must be limited. With typical BPFs found below 1000 Hz, it is essential that the control actuators have a good linear response in this region. To improve the response of the loudspeakers, each was enclosed separately within the computer casing by a small PVC enclosure. The enclosures were further optimized by the addition of a port, creating a traditional bass-reflex system (see Appendix A).

The 60-mm fan included seven blades and three support struts. It was run at a constant DC voltage, approximately 10 V, giving an approximate rotational speed of

5140 RPM giving a BPF of approximately 600 Hz. A small aluminum obstruction was also placed directly behind the fan to simulate possible stationary obstructions found in a computer casing. This obstruction had the effect of boosting the tonal component of the fan noise. An electronic infrared emitter/detector pair placed on either side of the fan was used to determine the BPF and served as a reference signal for the feed-forward adaptive control algorithm. It was essential that the reference signal contain the same frequency content as the noise to be controlled. The frequency spectrum of the signal received from the emitter/detector pair included the BPF and several harmonics. It was filtered once using a Krohn-Hite Model 3384 8-pole Butterworth high-pass filter at 500 Hz and twice with 8-pole Butterworth low-pass filters at 2000 Hz to isolate the first three harmonics of the BPF. These were the harmonics targeted for control.

Four Larson Davis 2551 half-inch Type-1 microphones were used as error sensor inputs for the control algorithm, with Larson Davis PRM426 preamplifiers. The preamplifiers were fed to a 12-channel PCB Piezotronics Model 483B07 ICP Signal Conditioner. The error sensor signals were high-pass filtered at 500 Hz using a Krohn-Hite Model 3364 4-pole Butterworth filter to eliminate low-frequency turbulence from airflow.

3.2 Control Source Configuration

The theory given in Chapter 2 suggested that three symmetrically spaced control sources should achieve control comparable to that of four symmetrically spaced control sources. A control system was thus manufactured with the 60-mm fan that employed three control sources to compare against results obtained with the four-source configuration. The arrangements of the two control systems are shown schematically in

Figure 3.4. An identical fan and identical control loudspeaker models were used for the three-source configuration. A removable top plate was machined for each configuration, to which the fan and loudspeakers were mounted. The top plate was then mounted in the same aluminum casing for both cases. The same separation distance, d = 0.045 m, was used between the fan and loudspeakers. The small aluminum obstruction was also used in both cases. Three Larson Davis 2551 half-inch Type-1 microphones were used as error sensor inputs for the control algorithm.

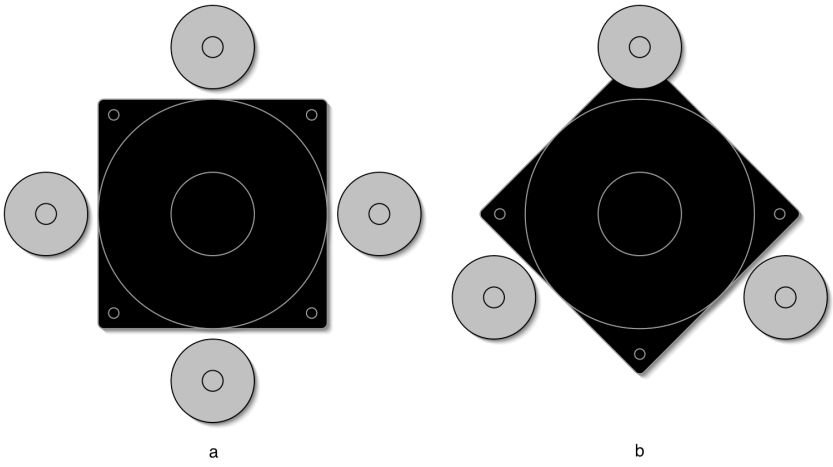

Figure 3.4 The 60-mm fan and speaker arrangement with (a) four control sources and (b) three control sources.

CHAPTER 4

RESULTS

4.1 Free-field Results

Free-field measurements of the systems were taken in an anechoic chamber. Figure 4.1 shows a rotating semicircular boom used in the chamber to measure the sound pressure level at equally spaced points away from the casing. The boom was 3.04 m in diameter, with thirteen Larson Davis half-inch Type-1 microphones placed at 15° increments around the boom. The boom was rotated clockwise in ten 18° increments to obtain a total of 130 data points over a complete hemisphere for each global sound pressure measurement. Data were acquired using a VXI-based Hewlett-Packard multi-channel dynamic signal analyzer with Data Physics SignalCalc analysis software.

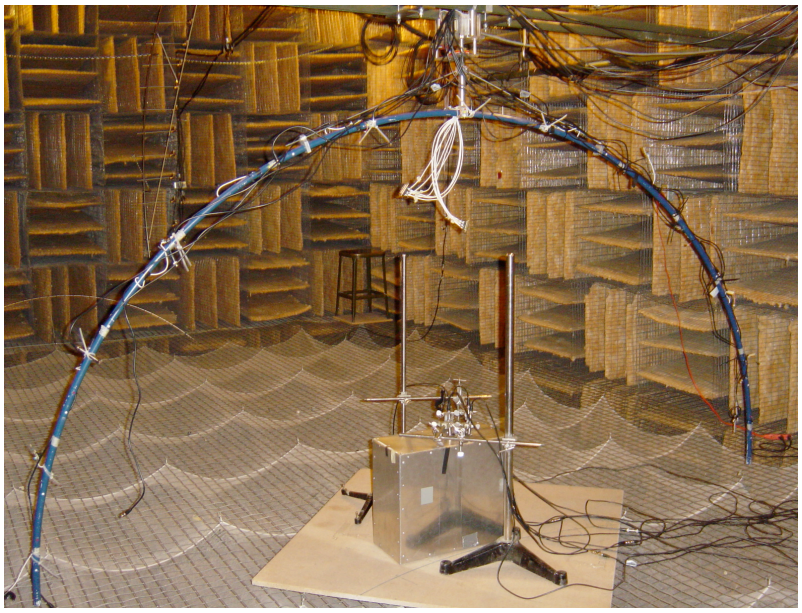

Figure 4.1 A rotating semicircular microphone boom in the anechoic chamber on the Brigham Young University campus.

The filtered-x LMS algorithm was implemented using a Spectrum 96000 floating-point digital signal processing (DSP) board, mounted in a computer with a 486 processor. The sampling frequency was 4 kHz for all measurements shown for the 60-mm system. The control outputs from the DSP were low-pass filtered at 2 kHz to prevent aliasing. The control system used 20 coefficients to estimate the control filter transfer function, $\mathbf{W}_n(z)$, and 16 coefficients for the control path transfer function, $\hat{\mathbf{H}}(z)$. The computer and DSP hardware were located in a control room separate from the anechoic chamber, so all measurements and control tests were performed remotely.

4.1.1 Four-Control Source Configuration

For the 60-mm fan, the BPF was 600 Hz. Figures 4.2 through 4.4 show plots of the reduction achieved for the first three harmonics of the system. For direct comparison to Gee's results, a spatially averaged global square pressure reduction (labeled mean-square pressure reduction, or MPR, by Gee and Sommerfeldt[8]) was calculated according to the formula

$$MPR(f) = 10\log\left(\frac{\sum_{n=1}^{N} p_{OFF}^2(x_n, f)}{\sum_{n=1}^{N} p_{ON}^2(x_n, f)}\right), \tag{4.1}$$

where N is the total number of data points measured and f represents the frequency of interest. The subscripts OFF and ON denote the pressure with active control off and active control on.

In the plots, the mesh surface corresponds to the sound pressure level of the fan radiating without active control, and the solid surface is the radiation with control running. The plots give global sound pressure level measurements in dB re 20 μPa, with increased pressure level indicated by both increasing spherical radius and color scale (for

control on). It is noted that the fan and control system are raised 0.45 m above the measurement hemisphere (see Figure 4.1), which leads to a slight skewing of the pressure levels toward the positive z-direction. For the first three harmonics, the control system achieved MPRs of 14.9 dB, 18.9 dB, and 10.5 dB, respectively. It is interesting to note that the mesh surface reveals the omni-directional behavior of the fan's BPF and harmonics, suggesting monopole-like characteristics.

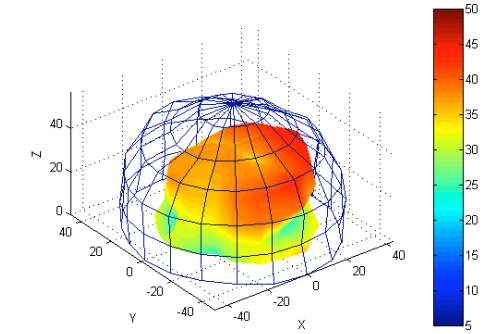

Figure 4.2 Sound pressure level in dB of the 60-mm fan noise at the fundamental frequency of 600 Hz with (color) and without (mesh) ANC. Control used four error sensors and four secondary sources. (Magnitude of values on X, Y, and Z axes indicate sound levels.)

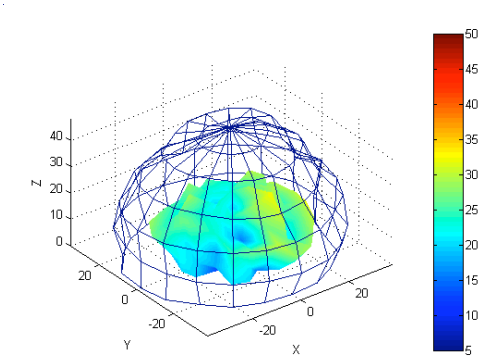

Figure 4.3 Sound pressure level in dB of the 60-mm fan noise at 1200 Hz with (color) and without (mesh) ANC. Control used four error sensors and four secondary sources. (Magnitude of values on X, Y, and Z axes indicate sound levels.)

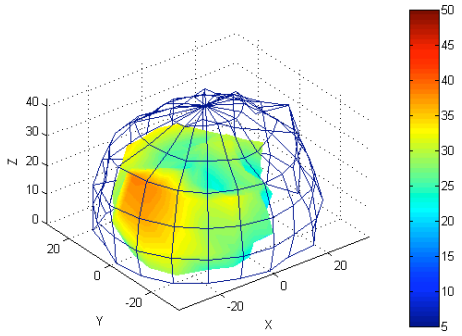

Figure 4.4 Sound pressure level in dB of the 60-mm fan noise at 1800 Hz with (color) and without (mesh) ANC. Control used four error sensors and four secondary sources. (Magnitude of values on X, Y, and Z axes indicate sound levels.)

Further calculations were made to attempt a closer estimate of sound power reductions for the 60-mm fan to compare with and validate the MPR results. The method used to obtain the sound power estimate followed a method similar to that described by Leishman *et al*.[17]

Because sound power is a measurement of acoustic intensity integrated over area, it is typically measured by arranging the measurement points such that they cover an equal area interval around the test source. As seen in Figure 4.5, the microphones were spaced equidistant on the semicircular boom at an angle θ_0 = 15 degrees. But the azimuthal rotation (ϕ_0 = 18 degrees) gave an increase in the ith measurement area created toward the bottom of the microphone boom. To compensate for this, sound power level over the hemisphere was calculated as

$$L_{\Pi} \approx 10 \log \left[\sum_{i=1}^{13} \sum_{n=1}^{10} A_i 10^{0.1 L_{pni}} \right], \tag{4.2}$$

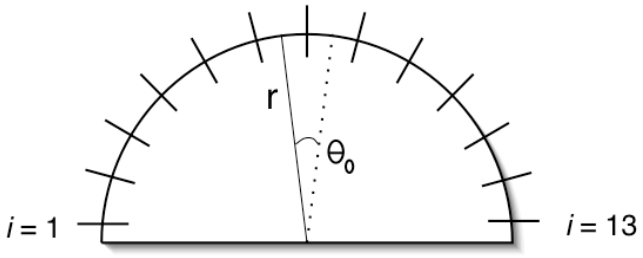

Figure 4.5 Diagram depicting microphone spacing on a semicircular microphone boom.

where L_{Pni} is the sound pressure level at the ith microphone position and the nth boom rotation position of a semicircle rotated 180 degrees. An area weighting function, A_i, was applied to each pressure measured at the ith microphone position located on a semicircle of radius r, defined by

$$A_i = \begin{cases} r^2\phi_0 \cos\theta_{i+1} & ; \quad i = 1 \\ r^2(\cos\theta_{i+1} - \cos\theta_i)\phi_0 & ; \quad 2 \le i \le 6 \\ 2\pi r^2(1 - \cos\frac{\theta_0}{2}) & ; \quad i = 7 \\ r^2(\cos\theta_i - \cos\theta_{i+1})\phi_0 & ; \quad 8 \le i \le 12 \\ r^2\phi_0 \cos\theta_i & ; \quad i = 13 \end{cases}, \tag{4.3}$$

with angles defined as

$$\begin{aligned} \theta_i &= \theta_0(i-7) - \tfrac{\theta_0}{2}, \\ \theta_0 &= 15°, \\ \phi_0 &= 18°. \end{aligned} \tag{4.4}$$

The radius r of the microphone boom was 1.52 m, which was in the acoustic far-field of the source. Sound power reductions calculated in this manner at the BPF, second, and third harmonics were 14.5 dB, 16.6 dB, and 9 dB, respectively. They were thus similar but less than the values calculated earlier for the global sound pressure level reductions.

The selection procedure for the error sensor locations used to achieve these results was based on the theory given in Chapter 2. Locations were initially chosen on the null

pattern corresponding to points that lay on the control plane null contour and were common for all harmonics of interest. These points were located near each control loudspeaker. Numerous locations near the ideal locations were used for testing and those giving the best results were implemented. The implemented locations are shown as red markers in Figure 4.6.

As can be seen, these locations correlated well with the predicted controlled pressure null. The locations were approximately 19 mm away from the outer edge of the fan. A need to have the error microphones sufficiently far from the fan was in part due to the excessive broadband noise found with locations closer to the fan. This was caused by airflow across the diaphragm of the microphone, and negatively affected the performance of the ANC system.

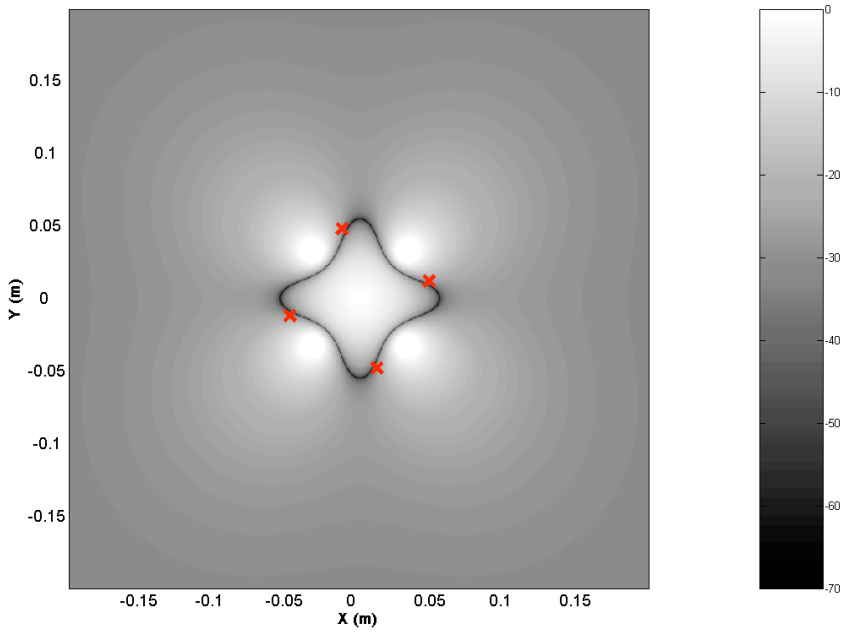

Figure 4.6 Control plane plot at 600 Hz for four secondary sources with the red markers indicating implemented error sensor locations.

4.1.2 Three-Control Source Configuration

Figures 4.7 through 4.9 show the resulting sound pressure reductions for the three-source configuration. The three-source control system achieved MPRs of 14.7 dB, 16.7 dB, and 6.9 dB for the first, second, and third harmonics, respectively. These reductions were slightly less than those calculated for the four-source system. The sound power reductions were 14.8 dB, 15.7 dB, and 8.5 dB, which were comparable (within 0.9 dB) to the sound power reductions calculated for the four-source system. Interestingly, the sound power reductions for the first and third harmonics were greater than the MPRs calculated for the three-source system.

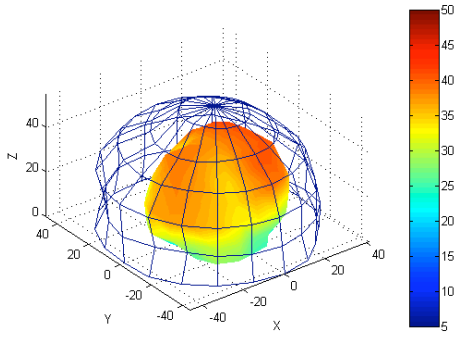

Figure 4.7 Sound pressure level in dB of the 60-mm fan noise at 600 Hz with (color) and without (mesh) ANC. Control used three error sensors and three secondary sources. (Magnitude of values on X, Y, and Z axes indicate sound levels.)

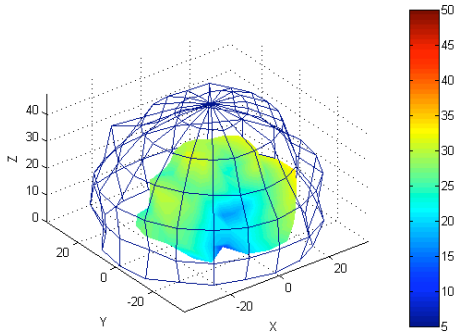

Figure 4.8 Sound pressure level in dB of the 60-mm fan noise at 1200 Hz with (color) and without (mesh) ANC. Control used three error sensors and three secondary sources. (Magnitude of values on X, Y, and Z axes indicate sound levels.)

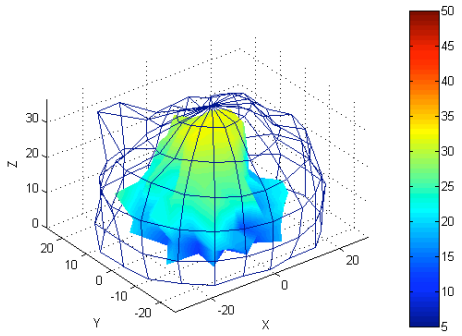

Figure 4.9 Sound pressure level in dB of the 60-mm fan noise at 1800 Hz with (color) and without (mesh) ANC. Control used three error sensors and three secondary sources. (Magnitude of values on X, Y, and Z axes indicate sound levels.)

The error sensor locations used for the three-control source system were selected as before, and are shown in Figure 4.10. This again shows good agreement with the predicted pressure null. These locations were approximately 21 mm away from the outer edge of the fan.

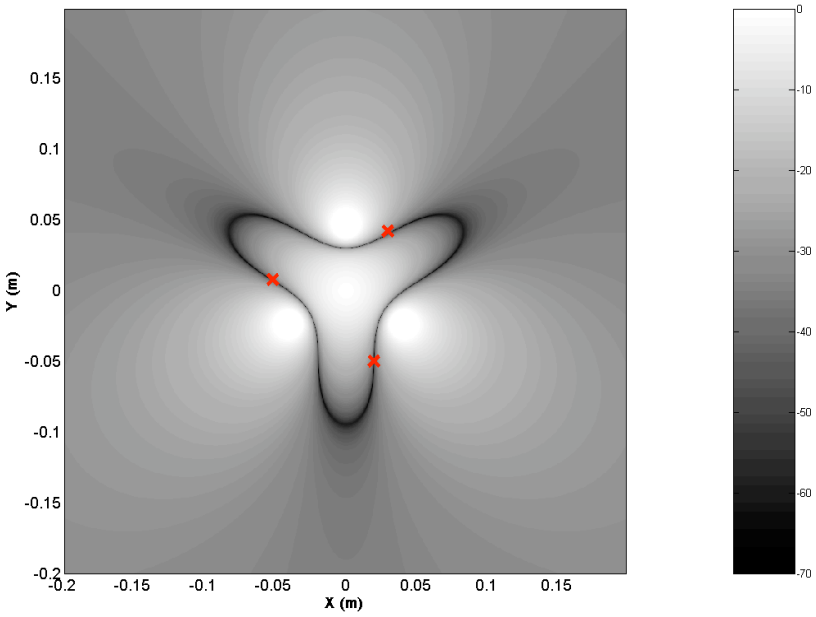

Figure 4.10 Control plane plot at 600 Hz for three secondary sources with the red markers indicating error sensor locations.

4.2 Reflective Environment

Because of the reflective nature of most environments containing axial cooling fans, a test of the robustness of the control system in a highly reflective environment was desired. The 60-mm control system with the four-control source configuration was moved to a reverberation chamber for a feasibility test in a worst-case scenario. The system was set up exactly as in the anechoic environment isolating the reflective environment as the control variable. The reverberation chamber was used to make sound power measurements according to ISO 3741.[18]

Thirty Larson Davis 2551 half-inch Type-1 microphones were used to input sound pressure to the VXI-based Hewlett-Packard multi-channel dynamic signal analyzer, with Data Physics SignalCalc analysis software. The control system was

moved to four separate locations in the middle of the reverberation room, and measurements were made at each location with and without the control system running. The sound power was calculated for the fan noise with and without ANC, and the difference calculated. To examine the effect of close approximation of reflective surfaces, the control system was then moved to one corner of the room so that the center of the fan was located approximately 0.2 m from each of the two adjoining reflective surfaces. Again, sound power was calculated for ANC off and ANC on, although this position went contrary to the standard.

Sound power reductions measured in the middle of the reverberation chamber were 10.4 dB, 15.3 dB, and 5.4 dB for the BPF, the second, and third harmonics, respectively. The sound power reductions calculated with the control system in the corner of the reverberation room were 10.6 dB, 8.8 dB, and 5.5 dB.

4.3 Discussion

Table 1 gives a comparison of the sound power reductions (SPR) achieved by all control configurations and environments tested, including the previously reported mean-square pressure reduction (MPR) results of the 80-mm system.[8] The theoretical ideal attenuation predicted for each case is also shown.

	80-mm (4-source)		60-mm (4-source)		60-mm (3-source)		60-mm (reflect.)	
	MPR	**Ideal**	**SPR**	**Ideal**	**SPR**	**Ideal**	**SPR**	**SPR (near)**
BPF	10.1	37.9	14.5	34.6	14.8	34.3	10.4	10.6
2 × BPF	16.1	25.4	16.6	21.9	15.7	21.4	15.3	8.8
3 × BPF	12.8	19.5	9.0	13.8	8.5	12.9	5.4	5.5

Table 4.1 Overall noise reduction comparison (in dB) of the 80-mm control system, the 60-mm control system with four sources and three sources, the 60-mm four-control source system in a reflective environment, and the theoretical ideal.

4.3.1 Fan Size

The 60-mm system demonstrated similar control performance to that of the 80-mm system. The 60-mm system was able to achieve global control of the first three harmonics of the fan BPF. It appears, however, that it did not achieve optimal control of the BPF. This is indicated by the considerable increase of attenuation from the BPF to the second harmonic, which does not agree with the predictions by Nelson *et al.*[12] An increase in frequency gives an increase in kd, which should decrease the possible attenuation by the control sources. It is apparent, then, that the fundamental is not being attenuated as much as is ideally possible. A comparison to the minimum power radiation plot (Figure 2.3) confirms that this is the case. The 600-Hz tone produces a kd value of 0.5, which predicts an attenuation of more than 30 dB in the ideal case.

It was suspected that the smaller reduction might be attributed to poor actuator low frequency response at 600 Hz. To verify this suggestion, a total harmonic distortion analysis was done. Results showed little harmonic distortion at the typical driving voltages of the control loudspeakers. Further investigation revealed that at the error

sensor signal the control system had attenuated the BPF very close to the broadband noise level, as seen in Figure 4.11, suggesting that the broadband noise floor at 600 Hz may be limiting the control achieved at that frequency. The noise attenuation at the error sensor at 600 Hz is seen to be nearly 25 dB. Because the theory suggests that this location should be a pressure null, it is not surprising that this value is much larger than the attenuation actually achieved in the far field.

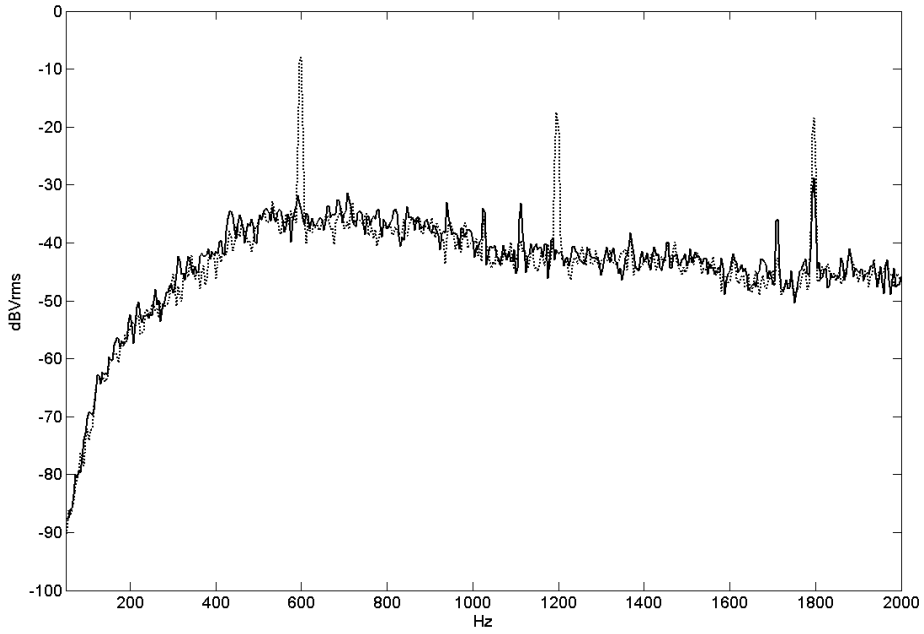

Figure 4.11 Typical error sensor spectrum for the 60-mm four-source configuration.

In the case of the second harmonic, attenuation at 1200 Hz (60-mm fan) was 0.5 dB greater than that reported for 740 Hz (80-mm fan). This comparison is not entirely accurate, as only MPR was calculated for the 80-mm system, and not SPR. Comparison of MPR for the two systems shows that the 60-mm system attenuated the sound field 2.8 dB more than the 80-mm system at the second harmonic. To compare to the theoretical

ideal for the second harmonic of the 60-mm fan, *kd* is calculated to be 1, giving a theoretical sound power attenuation of 21.9 dB, which is approximately 5 dB greater than that achieved experimentally. The SPL at 1200 Hz at the error sensor, however, is again seen in Figure 4.11 to be at the noise floor, as in the 600-Hz case.

A similar analysis follows for the third harmonic. In this case, however, the attenuation at 1110 Hz in the 80-mm system is 3.8 dB greater than at 1800 Hz in the 60-mm system (2.3 dB if comparing MPR). This may be expected, as the *kd* value increases from 1.2 for the 80-mm fan to 1.5 for the 60-mm fan at this frequency. Comparison to the minimum power radiation shows that the attenuation at 1800 Hz is again about 5 dB less than the theoretical ideal.

At the error sensor, the 1800-Hz tone was significantly attenuated, though not down to the noise floor as with the first two harmonics. This may be due, in part, to the processor speed and sampling rate used for the experiments. Snyder suggests that in order to achieve optimum active control, one should use a sampling rate that is at least 10 times the target frequency, but no more than 50 times the target frequency, though reasonable control has been shown with a sampling rate as low as three times the target frequency.[19] It is noted that in this case global control was exhibited at 1.8 kHz with a 4-kHz sampling frequency – a factor of just over two. This may have adversely affected the control performance, however, and may give explanation for the third harmonic not being attenuated to the noise floor, as were the first and second harmonics. While not yet achieving ideal values, reduction of the second and third harmonics in the 60-mm fan system appears to approach the predicted ideal.

4.3.2 Control Source Configuration

In both the three-source and four-source cases, the reduction at the BPF was around 14.5 dB – approximately 20 dB less than the predicted ideal for each case (see Figure 2.3). In Figure 4.12, a spectrum for the three-source error sensor is shown, again revealing that with ANC the BPF was attenuated to the broadband noise level. (The two uncontrolled peaks resulted from structural resonances of the computer casing and thus were not targeted with ANC in this experiment.)

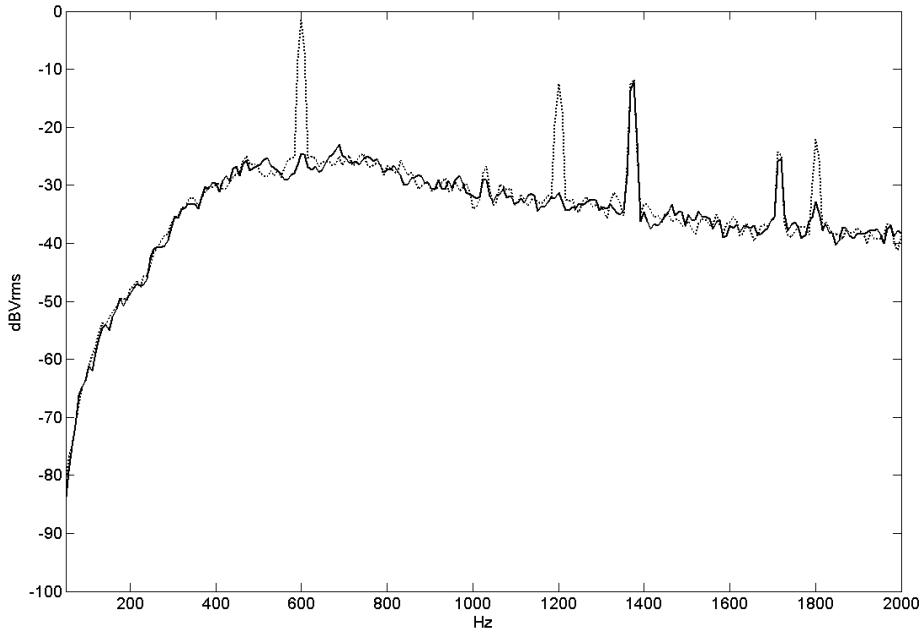

Figure 4.12 Typical error sensor spectrum for the 60-mm three-source configuration.

The second harmonic for the three-source control system achieved control comparable to that of the four-source system, with a 0.9 dB difference in favor of the four-source configuration. Again the control behavior was about 5 dB less than predicted (much closer to the ideal than for the BPF) and again the noise at the error sensor is down

to the broadband level. The third harmonic exhibited a slightly smaller deviation in the two control systems, showing only a 0.5 dB difference favoring the four-source system. Again, reduction is 4 to 5 dB less than predicted. The trends in all cases tend to follow the theory presented in Chapter 2.

4.3.3 Reflective Environment

The sound power results obtained in the reverberation chamber showed that ANC is in fact feasible in a highly reflective environment. The error sensor locations in the reverberation chamber were kept consistent with those used in the anechoic chamber measurements. Using this approach, however, did lead to a drop in performance at all harmonics. Comparison to the free-field environment showed that control performance dropped with the presence of the reflective surfaces by 4.1 dB for the BPF, 1.3 dB for the second harmonic, and 3.5 dB for the third harmonic. Close proximity of reflective surfaces appeared to introduce detrimental effects that may impair ANC further.

To begin an exploration of this drop in performance, the characteristics of the null pattern with the introduction of reflective surfaces were examined. Using a source imaging technique to represent reflective surfaces in the system, the error sensor location method given in Chapter 2 was extended to an environment including one and two reflective surfaces at varying distances. Image sources included images of both the fan noise source and the control sources. The reflective surfaces were given reflection coefficients of 1 (perfect reflection). Figures 4.13 through 4.18 show the results of the reflective surface modeling. In all the figures shown, the original noise source is located at the origin with the original control sources located at 45, 135, 225, and 315 degrees around the noise source. The solid vertical line represents the position of the inserted

surface. Reflections of all sources can be seen on the opposing side of the reflective surface(s).

The introduction of a single reflective surface is plotted in Figures 4.13 and 4.14 for 600 Hz and 1800 Hz, respectively. The most significant change in the nodal pattern can be seen on the side opposing the reflective surface, where the curvature is seen to extend perpendicular to the surface. More complex changes in nodal patterns are caused by additional reflective surfaces, as shown in Figures 4.15 through 4.18. (While none of the cases shown here replicate the ANC system placed in the center of the reverberation chamber, they are instructive in showing the effects of a reflective environment on the controlled pressure field.)

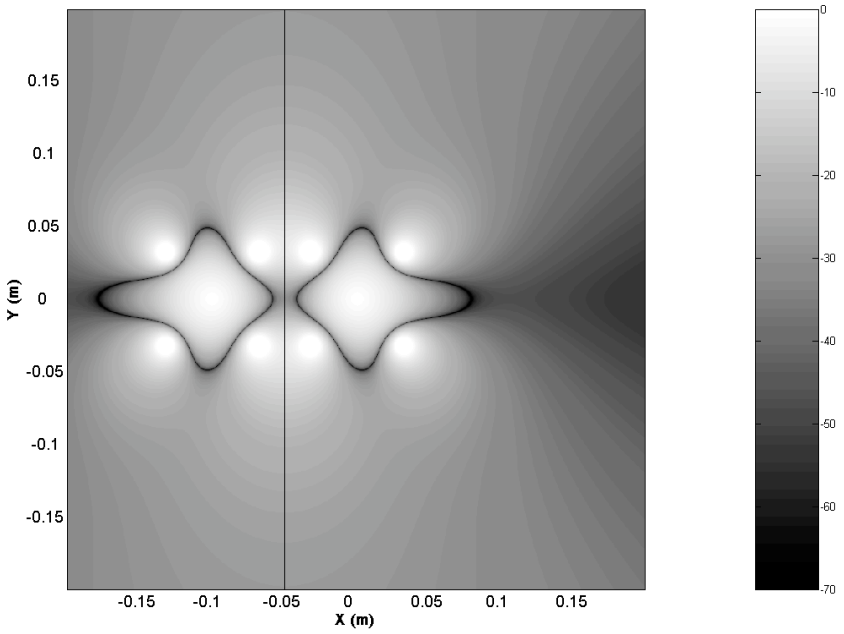

Figure 4.13 Controlled pressure field coplanar to the noise source and four secondary sources with one reflective surface – 600 Hz.

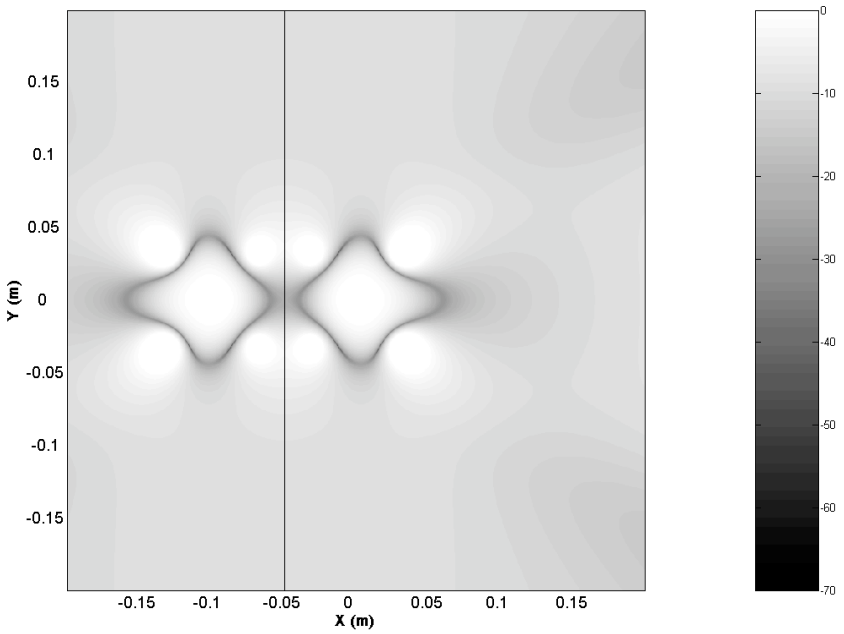

Figure 4.14 Controlled pressure field coplanar to the noise source and four secondary sources with one reflective surface – 1800 Hz.

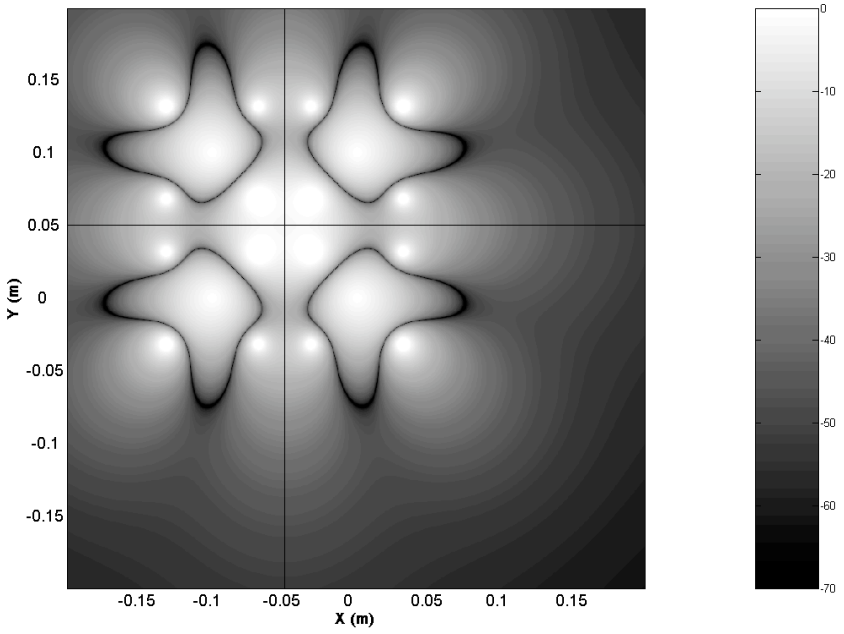

Figure 4.15 Controlled pressure field coplanar to the noise source and four secondary sources with two reflective surfaces – 600 Hz.

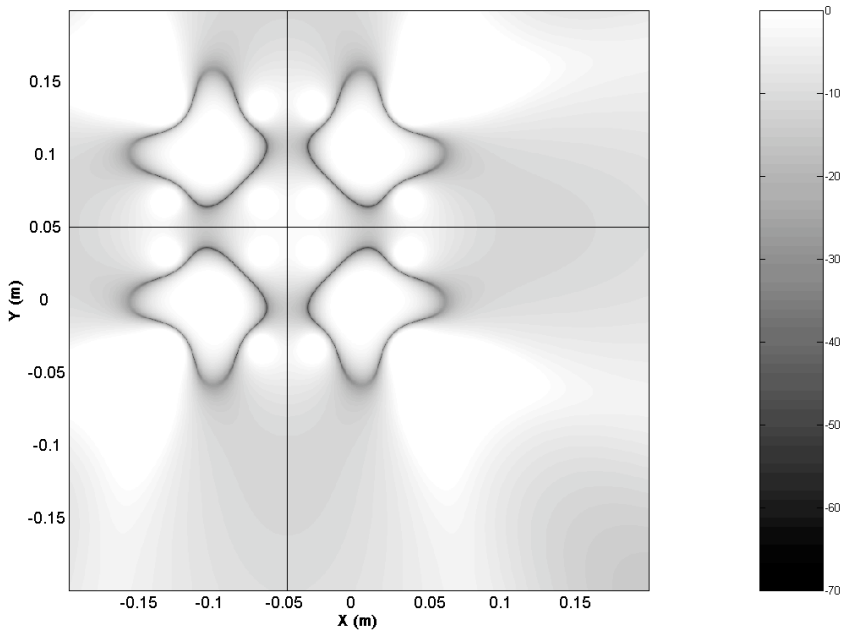

Figure 4.16 Controlled pressure field coplanar to the noise source and four secondary sources with two reflective surfaces – 1800 Hz.

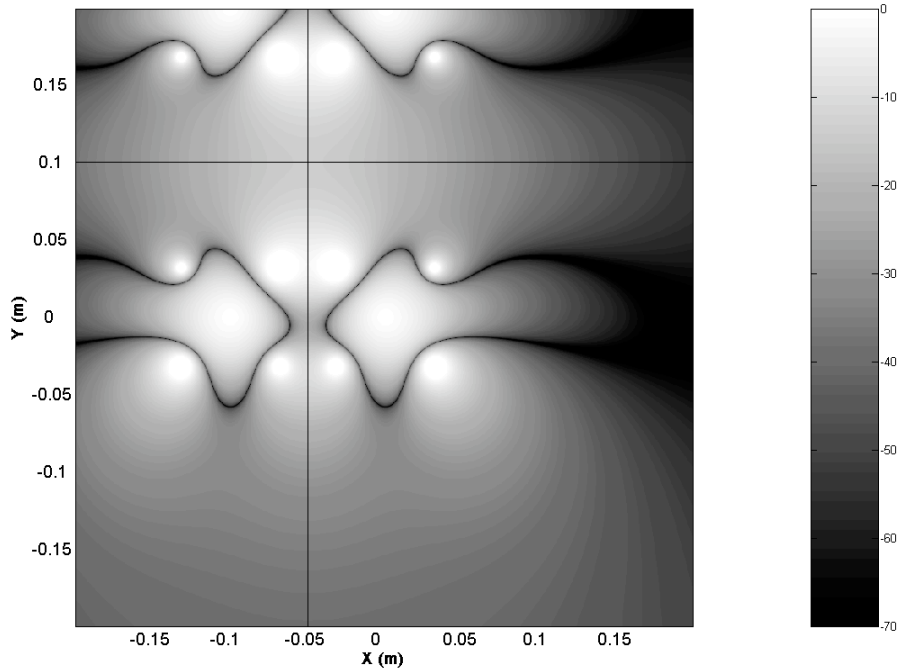

Figure 4.17 Controlled pressure field coplanar to the noise source and four secondary sources with two non-equidistant reflective surfaces – 600 Hz.

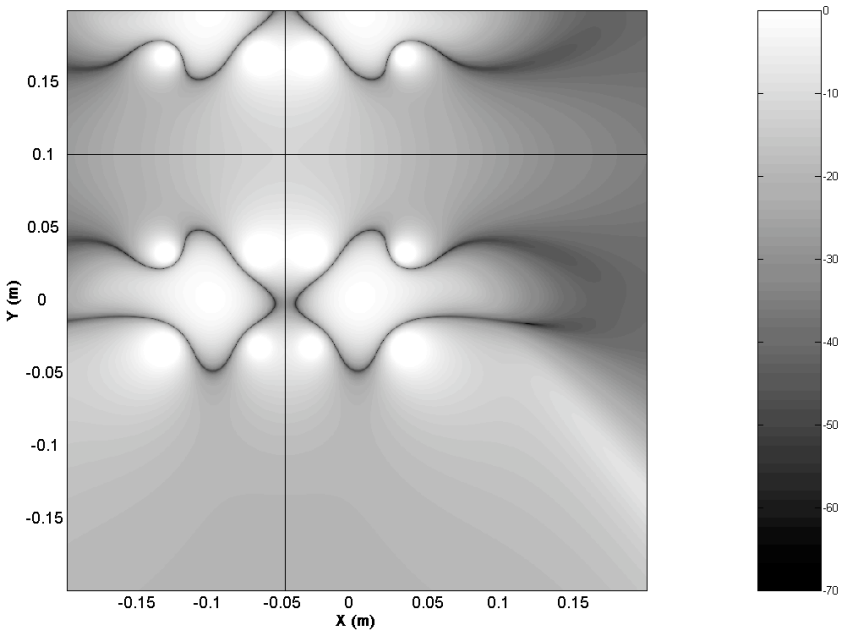

Figure 4.18 Controlled pressure field coplanar to the noise source and four secondary sources with two non-equidistant reflective surfaces – 1200 Hz.

It is apparent that the introduction of reflective surfaces affects the pattern of the pressure null on the control plane. This may have contributed to the decrease in control performance of the system when placed in the center of the reverberation chamber. The extent to which it may have affected the error sensor locations is unknown because of the distance of the reflective surfaces from the fan (ISO 3741 calls for a separation distance of at least 1 m between the sound source and any reflective surface). Such a distance from any reflective surfaces may possibly have had little to no effect on the null pattern. A further explanation may be found in the fact that the analysis of the multiple control configurations assumed a free field and did not account for nearby reflections. The reflective surfaces may have decreased the possible attenuation for the optimally

controlled case by increasing the overall energy in the system. This characteristic would likely be pronounced in experimental testing.

The ANC system placed in the corner of the reverberation chamber exhibited a large drop in attenuation achieved at the second harmonic of the BPF. The control plane of the system in the corner at 1200 Hz was simulated and is shown in Figure 4.19. Reflective surfaces are located at x = -0.2 m, and y = 0.2 m. The locations of the error sensors are again shown in red. It was suspected that the error sensor locations were changed significantly from the free-field case, but this did not appear to be so. Rather, the error sensors were located near positions that should have led to significant attenuation.

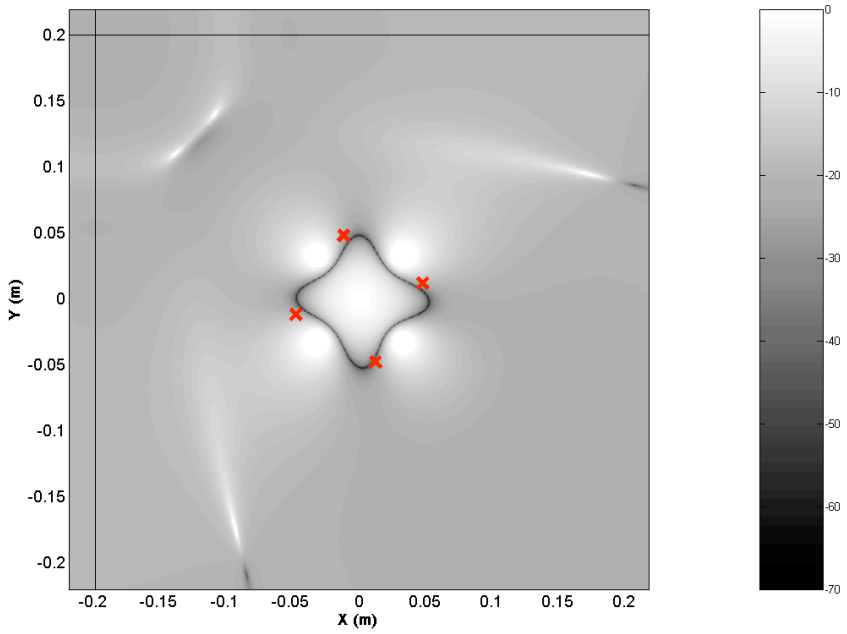

Figure 4.19 Control plan plot at 1200 Hz for four secondarysources with two reflective surfaces (reflective surfaces are located at x = -0.2 m and y = 0.2 m).

One possible explanation for the decrease in performance at 1200 Hz was that the effects of the reflections were much more prevalent at this distance. For example, it may

have been possible that traveling waves normally encountered in the free-field could have interfered sufficiently to develop standing wave patterns. If a standing wave were created, a node would exist at a distance approximately three quarters of a wavelength away from either or both nearby reflective surfaces. This distance at 1200 Hz is 0.2125 m. This could have disturbed control performance in that region. (No effect of this kind is seen in the image source simulations, however.)

Perhaps a reasonable explanation for the drop in sound power is simply the violation of the sound power measurement procedure with the control system in the corner. For standard measurements the source under test must be located at least one meter away from any reflective surface. As stated earlier, this was not the case. Also, the standard sound power measurements required four different positions of the source in the reverberation chamber. The mean of the four tests is then calculated. Because the control system in the corner was intended as a case study, only one measurement was taken. This may give reason for the discrepancy in the values calculated.

CHAPTER 5

CONCLUSIONS

5.1 Summary

The 60-mm fan control system appears to exhibit similar control performance to that of the 80-mm fan control system developed by Gee and Sommerfeldt.[8] This suggests that replacement of an 80-mm fan with a 60-mm fan and control system is a feasible step toward making active control a more practical method of reducing axial cooling fan noise. With the 60-mm fan and control actuator configuration meeting the spatial constraint of an 80 × 80 mm area, the need for manipulation of current electronic equipment design is minimal.

The performance of the three-source control configuration is comparable to that of the four-source configuration, and is therefore a feasible substitution where the geometry may be more conducive to implementation. Advantages of using only three secondary sources include a decrease in cost of parts, and a decrease of computational cost, with only a slight decrease in control performance.

Global active control was maintained in an environment with highly reflective surfaces without alteration made to the control system. Though a drop in control performance was seen, the ANC system would appear to be effective in an office environment with surfaces that are highly reflective. Approximation of these surfaces will determine in some part the amount of noise attenuation achieved by the control system. Theory suggests that a reliable method of error sensor placement may exist, if the surface locations are known a priori.

While not yet ideal, the experimental work performed on the 60-mm control system appears to support the theoretical work of Nelson, Hansen, and others on the analysis of multiple control source geometry effects in ANC. This research has also shown that implementation of ANC on a cooling fan application need not be cumbersome for a manufacturer that is wary of sacrificing space in electronic equipment. A further contribution was the validation that ANC of cooling fans is feasible in an office setting.

Concerning the placement of error sensors, the far-field null was found to achieve greater pressure attenuation than the near-field null, and would therefore lead to greater overall sound power attenuation. This may further explain why the experimentation does not yet achieve the ideal values. If placement of the error sensors in the far-field is feasible for a given application, doing so may lead to attenuation closer to the ideal predictions.

5.2 Recommendations for Future Work

Improvements upon the system are recommended for future research. For this work, limitations on the processor constrained the sampling frequency to 4 kHz. As explained in Section 4.3.1, this may have adversely affected control performance, particularly at the third harmonic. Employment of a faster processor should allow for more rapid computation and a higher sampling rate, and, with this change, better control of more harmonics of the BPF might be achieved.

The changes in the controlled field null pattern behavior require further experimentation. This includes the effects of near-field reflective surfaces, as well as the pattern change away from the control plane. An experimental study of the null patterns shown earlier would aid in proper selection of error sensor locations for different

applications where either reflective surfaces are present, or where an error sensor location away from the control plane is feasible and more convenient.

This research has not yet attempted to control the broadband component of the fan noise. As sufficient control of the tonal noise is demonstrated, the broadband noise becomes dominant. Efforts should be focused on attenuating the broadband noise component by using either active or passive means of control, or both.

The issue of airflow has not been thoroughly addressed. Airflow may be obtained by use of a plenum and a standardized fan performance curve. A plenum was originally constructed according to ISO 10302[20] (at half-scale) for this purpose. The fan curve depicts the aerodynamic characteristics of a fan by giving static pressure as the ordinate and airflow as the abscissa. With a given static backpressure, the airflow is available from the fan curve for a rated voltage. Fan curves vary with differing voltage, however, and must be determined by use of a standardized flow bench. Because of the change in driving voltages for the fans used in this research, the fan curves published by Mechatronics could not be used. A flow bench was not purchased nor manufactured for this research because of the expense.

Rudimentary measurements were made using a small wind meter to measure the wind speed directly in front of the fan and multiplying this value by the area of the fan. While some variation existed, this method indicated that the 60-mm fan achieves approximately 85-90% of the airflow of the 80-mm fan at the fan speeds used in this research. Acquisition of a flow bench is recommended for an accurate comparison of airflow for the different cooling fans, including a comparison of airflow with and without ANC operating.

REFERENCES

1. G. W. Evans and D. Johnson, "Stress and open-office noise," J. Applied Psychology **85**, 779-783 (2000).
2. P. Lueg, "Process of Silencing Sound Oscillations" (U.S. Patent No. 2,043,416, 1936).
3. H. F. Olson and E. G. May, "Electronic Sound Absorber," J. Acoust. Soc. Am. **25**, 1130-1136 (1953).
4. D. A. Quinlan, "Application of active control to axial flow fans," Noise Control Eng. J. **39**, 95-101 (1992).
5. M. Q. Wu, "Active cancellation of small cooling fan noise from office equipment," Proc. INTER-NOISE 95, edited by Robert J. Bernhard and J. Stuart Bolton, **2**, 525-528 (1995).
6. G. C. Lauchle, J. R. MacGillivray, and D. C. Swanson, "Active control of axial-flow fan noise," J. Acoust. Soc. Am. **101**, 341-349 (1997).
7. K. Homma, C. Fuller, and K. X. Man, "Broadband Active-Passive Control of Small Axial Fan Noise Emission," Proc. NOISE-CON 2003, nc03_123, 10 pages (2003).
8. K. L. Gee and S. D. Sommerfeldt, "A compact active control implementation for axial cooling fan noise," Noise Control Eng. J. **51**, 325-334 (2003).
9. S. D. Sommerfeldt, "Multi-channel adaptive control of structural vibration," Noise Control Eng. J. **37**, 77-89 (1991).
10. L. Huang and J. Wang, "Acoustic analysis of a computer cooling fan," J. Acoust. Soc. Am. **118**, 2190-2200 (2005).

11. K. D. Kryter, and K. S. Pearsons, "Judged Noisiness of a Band of Random Noise Containing an Audible Pure Tone," J. Acoust. Soc. Am. **38**, 106-112 (1965).

12. P. A. Nelson and S. J. Elliott, *Active Control of Sound*, Academic Press, London, 1992.

13. C. H. Hansen and S. D. Snyder, *Active Control of Noise and Vibration*, E & FN SPON, London, 1997.

14. K. L. Gee and S. D. Sommerfeldt, "Application of theoretical modeling to multichannel active control of cooling fan noise," J. Acoust. Soc. Am. **115**, 228-236 (2004).

15. K. L. Gee, "Multi-channel active control of axial cooling fan noise," MS thesis, Brigham Young University, Provo, UT, 2002.

16. T. W. Leishman, Private Communication, Provo, UT, July, 2006.

17. T. W. Leishman, S. Rollins, and H. M. Smith, "An experimental evaluation of regular polyhedron loudspeakers as omnidirectional sources of sound," J. Acoust. Soc. Am. (in process).

18. *Acoustics—Determination of sound power levels of noise sources using sound pressure – Precision method for reverberation rooms,* International Standard ISO 3741, International Organization for Standardization, Geneva, Switzerland, 1999.

19. S. D. Snyder, "Microprocessors for active control: Bigger is not always enough," Proc. Active 99, 45-62 (1999).

20. *Acoustics—Method for the measurement of airborne noise emitted by small air-moving devices,* International Standard ISO 10302, International Organization for Standardization, Geneva, Switzerland, 1996.

21. T. W. Leishman, Physics 562 Lecture Notes, Brigham Young University, 2004.

22. L. E. Kinsler, A. R. Frey, A. B. Coppens, and J. V. Sanders, *Fundamentals of Acoustics* 4th Edition, John Wiley & Sons, New York, 2000.

23. R. H. Small, "Vented-box loudspeaker systems, part 2: large-signal analysis," J. Audio Eng. Soc. **21**, 438-444 (1973).

APPENDIX A

Four LASCO 3/4-inch PVC pipe end caps were used for the miniature loudspeaker enclosures (though rated for 3/4-inch PVC pipe, the actual end cap inside diameter was 1 1/16 in., or 27 mm). To optimize the loudspeaker enclosures, a small port was added to each enclosure to be tuned as a Helmholtz resonator. The PVC effective enclosure volume was measured to be $V = 13.6 \times 10^{-6}$ m^3. This effective volume was the volume of the enclosure minus the volume displacement of the miniature driver. The port was to be drilled in the aluminum plate, giving a port length of l = 2.38 mm. Treating the volume as an acoustic compliance, C_A, and the port as an acoustic mass, M_A, the resonance frequency of the box was tuned to 600 Hz (the BPF) according to[21]

$$f_B = \frac{1}{2\pi}\sqrt{\frac{1}{M_A C_A}}, \tag{A.1}$$

where

$$M_A = \frac{\rho l'}{S}, \tag{A.2}$$

and

$$C_A = \frac{V}{\rho c^2}. \tag{A.3}$$

S is the cross-sectional area of the port, and l' is the effective port length,[22]

$$l' = l + 2 \times 0.85a, \tag{A.4}$$

where a is the radius of the port.

The optimum port diameter resulting from the previous calculations was 3.3 mm. It is noted that this diameter does not satisfy the general guideline given by Small[23] for minimum port diameter size to avoid spurious noise generation with large signal

amplitudes. It was anticipated that the signals would be sufficiently small to avoid noise produced by a large volume velocity.

Total harmonic distortion (THD) was measured for a 600 Hz input signal at several voltages for the loudspeakers used in the 60-mm control system without ports, and can be seen in Figure A.1. The maximum driving voltages measured for the loudspeakers when controlling the fan noise were 0.6 Vrms. This corresponds most closely to a 0.9 Vpk driving voltage shown in the third plot.

An experimental baffled loudspeaker was then used to test different port diameters so that the optimum port diameter could be chosen. The experimental enclosure included port diameters of 1 mm, 2 mm, 3 mm, and 4 mm. THD measurements were taken with each port incorporated individually, and then with several combinations of ports. The best result was obtained using a 3-mm port in combination with a 1-mm port, resulting in two ports for the enclosure. The total surface area for this combination was 31.4×10^{-6} mm^2 which was extremely close to the surface area of 34.2×10^{-6} mm^2 for the predicted 3.3-mm diameter hole. Figure A.2 shows the THD measurements for this combination. The test loudspeaker with the port exhibited considerably less harmonic distortion at the higher driving voltages than the control loudspeaker used previously.

Incorporating the ports with the loudspeaker enclosures significantly decreased the driving voltage required to control the fan noise. This allowed for extensive use of the sensitive miniature loudspeakers and decreased chances of over-driving them. However, no significant change in the resultant control behavior was seen.

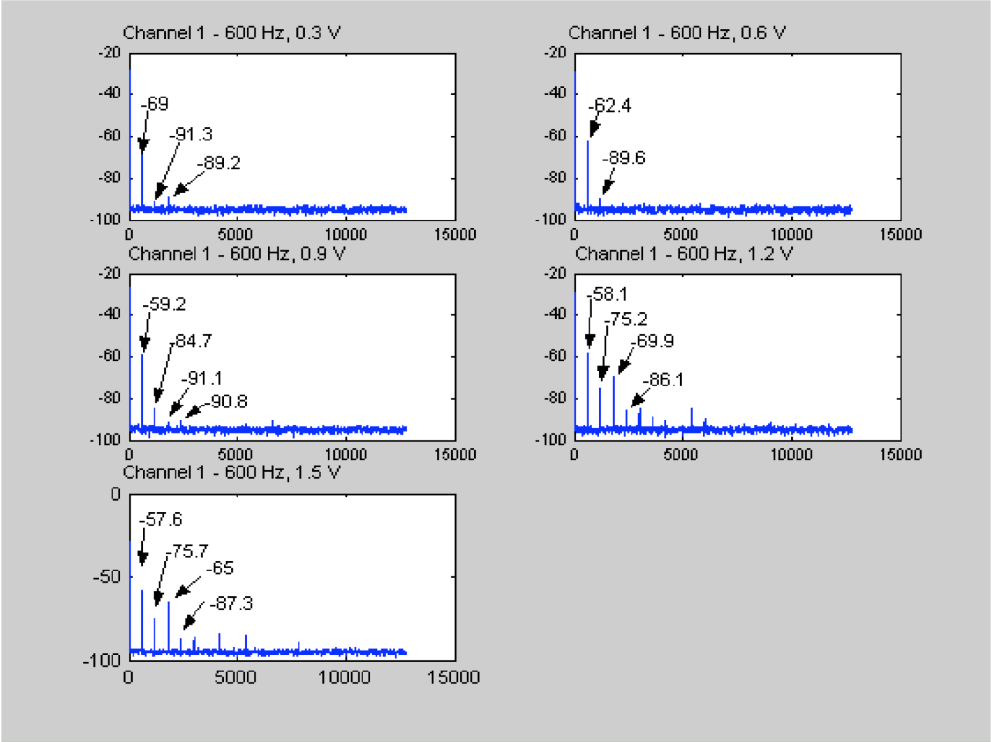

Figure A.1 THD measurements for a control loudspeaker without the port.

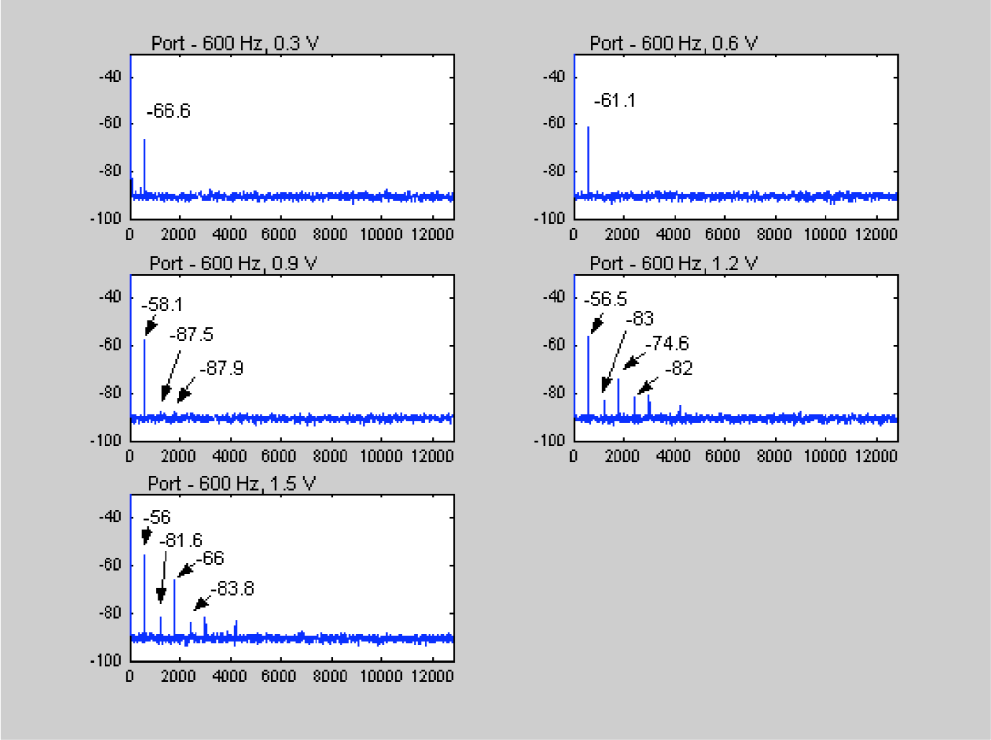

Figure A.2 THD measurements for a test control loudspeaker with the port.